Chapter 8
Upper Atmosphere and Ionosphere of Saturn

Andrew F. Nagy, Arvydas J. Kliore, Michael Mendillo, Steve Miller, Luke Moore, Julianne I. Moses, Ingo Müller-Wodarg, and Don Shemansky

Abstract This chapter summarizes our current understanding of the upper atmosphere and ionosphere of Saturn. We summarize the available observations and the various relevant models associated with these regions. We describe what is currently known, outline any controversies and indicate how future observations can help in advancing our understanding of the various controlling physical and chemical processes.

8.1 Introduction

The direct exploration of the upper atmosphere and ionosphere of Saturn began nearly 30 years ago with the flyby of the Pioneer 11 spacecraft (September 11, 1979), followed shortly by Voyagers 1 and 2 (November 12, 1980 and August 26, 1981, respectively). These flybys offered us a glimpse of Saturn, which, combined with earlier ground based and remote measurements from Earth orbit, did provide some basic ideas on the temperature and composition of the upper

A.F. Nagy
Department of Atmospheric Ocean and Space Sciences,
University of Michigan, Ann Arbor, MI, 48109, USA

A.J. Kliore
Jet Propulsion Laboratory, California Institute of Technology,
Pasadena, CA, 91109, USA

M. Mendillo and L. Moore
Center for Space Physics, Boston University, Boston, MA,
02215, USA

S. Miller
Department of Physics and Astronomy, University College, London,
WC1E 6BT, UK

J.I. Moses
Lunar and Planetary Institute, Houston, TX, 77058, USA

I. Müller-Wodarg
Space and Atmospheric Physics, Imperial College London,
London, SW7 2AZ, UK

D. Shemansky
Planetary and Space Science Division, Space Environment
Technologies, Pasadena, CA, 91107, USA

atmosphere and on ionospheric electron densities. The information on the thermosphere and ionosphere during the Pioneer and Voyager flybys came from two sources: the UV spectrometer and radio occultation observations. Since the insertion of Cassini into orbit around Saturn, the amount of data has very significantly increased, although still only the same two observation techniques provide most of the information on the upper atmosphere and ionosphere. However the quality of these measurements, as well as the spatial and temporal coverage, are significantly enhanced with Cassini. In this chapter we summarize our current understanding of the upper atmosphere and ionosphere of Saturn based on spacecraft and ground based measurements and modeling activities. Some of the other chapters (e.g., Chapter 12) are somewhat associated with the topics to be discussed here.

8.2 Structure and Composition of the Neutral Upper Atmosphere

In this chapter, we are defining the upper atmosphere to be the region above the "homopause" level, which is the altitude level at which molecular diffusion begins to dominate over eddy mixing. Below the homopause, atmospheric motions act to keep the atmosphere well mixed such that the mole fractions of chemically inert species do not vary significantly with altitude. Above the homopause, vertical diffusive separation of the species occurs, and the density of each neutral species drops off with altitude with its own scale height determined by its molecular mass (assuming no sources or sinks). Species much more massive than H and H_2 drop off precipitously with altitude above the homopause region, allowing for a convenient division between the middle and upper atmosphere. Saturn's upper atmosphere above the homopause is dominated by the least massive species H_2, H, and He.

Rate processes in the photochemistry of the thermosphere depend critically on the extent of the departure of the H_2 ground state, H_2 X(v:J), from local thermodynamic equilibrium (LTE). In earlier works (see Yelle and Miller 2004;

Strobel 2005 for reviews) the H_2 X(v:J) energy states have not been explicitly calculated, leaving rate processes highly uncertain. A competent approach requires calculation at the discrete rotational level using a solar emission model at resolutions of order 500,000 $(\lambda/\Delta\lambda)$. Such a calculation has been done by Hallett et al. (2005a,b) (see Killen et al. 2009 for details of the solar model), but some critical rate processes are not definitively established at this time, and thus even the more complete recent calculations have significantly underestimated the excited vibrational populations in H_2 X(v:J) compared to observation (Hallett et al. 2005b). Ionospheric processes depend on the state of H_2 X(v:J), and whether or not H_2O is assumed to be present as an inflowing component of significance in the thermosphere (see Section 8.6).

The Cassini Ultraviolet Imaging Spectrometer (UVIS) experiment (Esposito et al. 2004) provides the most accurate platform to date for extracting information on the neutral upper-atmospheric structure and composition of a giant planet, primarily because of the higher spectral resolution, signal rates, and dynamic range as compared with previous instruments. The Cassini UVIS experiment has supplied data on the atmospheric physical properties of Saturn through three observational programs: (1) solar and stellar occultations in the EUV/FUV range that allow extraction of vertical profiles of H_2 and hydrocarbon abundances from the top of the atmosphere to about 300 km above the 1 bar pressure level, (2) dayglow spectral images, which together with the ultraviolet occultation results and with constraints from the Cassini radio science measurements of ionospheric and atmospheric structure, constrain model calculations and provide atmospheric properties, and (3) images of the magnetosphere that show the escape profile of atomic hydrogen from the top of the Saturn atmosphere.

8.2.1 Determination of Atmospheric Properties from Ultraviolet Occultations

Absorptive occultations have provided much information on the structure and composition of the upper atmosphere of Saturn (e.g., Atreya et al. 1984; Smith and Hunten 1990). In such observations, the Sun or a UV-bright star provides a source of ultraviolet light that is monitored as the source passes behind the planet as viewed from a detector. Vertical profiles of temperature and the concentration of atmospheric constituents can be obtained from analysis of the observed attenuation of the light as a function of wavelength and radial distance from the planet's center. Six ultraviolet occultation experiments were performed during the encounters of the Voyager 1 and 2 spacecraft with Saturn; the results of those

occultations are described in Broadfoot et al. (1981), Sandel et al. (1982), Festou and Atreya (1982), Smith et al. (1983), and Vervack and Moses (2009). To date 15 stellar occultations have been obtained by the Cassini UVIS instrument over a range of latitudes from about 43° to −50°, and 7 solar occultations have been obtained over a range of latitudes from about 66° to −60°. The results from the UVIS occultation of the star δ-Ori on day-of-year (DOY) 103 of 2005 obtained at a latitude of −42.7° are presented here and in more detail in Shemansky et al. (2009) and Shemansky and Liu (2009). The temperature profile obtained from the occultation of ζ-Ori on DOY 141 in 2006, corresponding to a latitude of 15.2° is also presented in this section.

For the Cassini UVIS occultations, the H_2 component is obtained in the EUV Channel through forward modeling of the transmission spectrum using accurate temperature dependent cross sections (Hallett et al. 2005a, b; Shemansky and Liu 2009). The transmission spectra are fitted using separate vibrational vectors of the ground state H_2 X(v:J) structure. Details of the H_2 physical properties are described by Hallett et al. (2005a, b) for the non-LTE environment that develops in the excited atmosphere. The atmospheric temperature is derived through both iterative determination of rotational temperature and through the shape of the vertical H_2 density distribution in the hydrostatic model calculations (Shemansky and Liu 2009). At lower altitudes the kinetic temperature is also constrained by the measurements of the absorption structure of the C_2H_2 diffuse temperature sensitive $(\tilde{C} - \tilde{X})$ bands (Shemansky and Liu 2009; Wu et al. 2001).

Figure 8.1 shows the preliminary forward modeled hydrostatic vertical density distributions from the Shemansky and Liu (2009) analysis of the UVIS δ-Ori stellar occultation on 2005 DOY 103 at a dayside latitude of −42.7°; the model is anchored in the 0–400 km region using the Lindal et al. (1985) radio-occultation results. Shemansky and Liu (2009) have also reanalyzed the Voyager 2 (V2) UVS δ-Sco stellar egress occultation using the H_2 model described above, and the resulting vertical H_2 profile is included in Fig. 8.1. The Voyager 2 δ-Sco egress occultation (Smith et al. 1983; Vervack and Moses 2009) occurred on the darkside at a latitude of 3.8°. The differences in H_2 density at a given altitude evident in Fig. 8.1 are mainly the consequence of the different gravitation scales adopted at the different latitudes of the two occultations (Shemansky and Liu 2009). Figure 8.1 also shows the modeled helium distribution anchored at a [He]/[H_2] = 0.12 mixing ratio at 1 bar (Shemansky and Liu 2009). The [He]/[H_2] mixing ratio affects the modeled temperature structure in the vicinity of the mesopause, which is in turn constrained by the temperature dependence of the C_2H_2 $(\tilde{C} - \tilde{X})$ band cross section, such that an upper limit to the [He]/[H_2] mixing ratio can be obtained (Shemansky and Liu 2009). In the upper

Fig. 8.1 Plot of density versus altitude obtained from forward modeling of the Cassini UVIS δ-Ori stellar occultation on 2005 DOY 103 at a latitude of −42.7° (Shemansky and Liu 2009). Density values derived from the Voyager 2 UVS δ-Sco stellar egress occultation observations at 3.8° are also shown for comparison. The overplotted light lines indicate the altitude range over which meaningful constraints can be obtained from the measured data. The magenta curve is total density from the CIRS results (Fletcher et al. 2007), after converting their pressures to densities using a hydrostatic equilibrium model
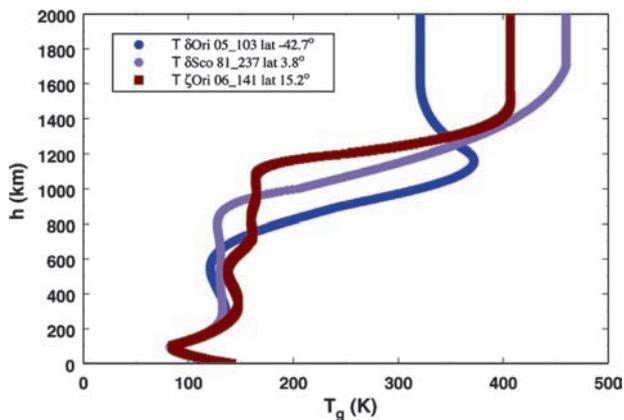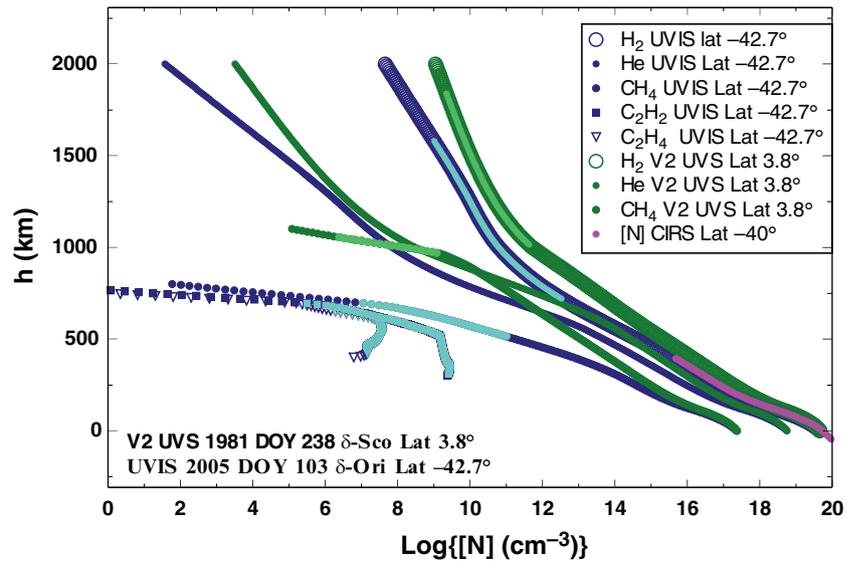
Fig. 8.2 Derived vertical temperature profiles from the Cassini UVIS occultations of δ-Ori (latitude −42.7°, 05 DOY 103) and ζ-Ori (latitude 15.2°, 06 DOY 141) and from the Voyager occultation of δ-Sco (latitude 3.8°, 81 DOY 237). These results are obtained using a common H_2 physical model (Shemansky and Liu 2009)

thermosphere, density and temperature vertical profiles evidently have a significant dependence on latitude (Shemansky and Liu 2009) (see Fig. 8.2), and the UVIS 2006 ζ-Ori occultation at 15.2° latitude has a similar vertical profile to the Voyager δ-Sco result (at 3.8° latitude) above 1,000 km (Shemansky and Liu 2009).

The UVIS FUV spectrograph stellar occultation data also lead to information on the hydrocarbon concentrations of CH_4, C_2H_2, and C_2H_4, as shown in Fig. 8.1. The evidence for other species in the transmission spectra is discussed by Shemansky and Liu (2009). In contrast, the only hydrocarbon profile that can be reliably extracted from the Voyager 2 δ-Sco stellar egress occultation is that of CH_4 (Shemansky and Liu 2009; Vervack and Moses 2009) (see Fig. 8.1). The methane homopause is just above 600 km in

the UVIS occultation and at ∼900 km in the Voyager 2 occultation, assuming the same oblate-spheroid model as used in the Cassini navigation package to define the zero altitude level at the 1-bar radius as a function of latitude (Shemansky and Liu 2009). Although the vertical displacement of the hydrocarbon homopause levels in the two cases is partially explained by the vertical displacement of the H_2 densities (see Fig. 8.1), a real difference in the location of the homopause in H_2-density space or pressure space does appear to exist, with the Cassini data implying a methane homopause located at higher pressures or H_2 densities than was the case for any of the six Voyager occultations (see Section 8.3 and Vervack and Moses 2009).

The derived temperature profiles from the UVIS 2005 δ-Ori, the UVIS 2006 ζ-Ori occultation, and the Voyager 2 1981 δ-Sco egress occultation (Shemansky and Liu 2009) are shown in Fig. 8.2. The preliminary UVIS results at −42.7° latitude shows a distinct mesopause at 545 km at a temperature of 121 K. The mesopause temperature is limited by the measured structure of the C_2H_2 $(\tilde{C} - \tilde{X})$ bands. The hydrostatic model calculation of the structure confined by the measured H_2 profile at higher altitudes, and the Voyager radio occultation results at altitudes below 400 km, is dependent on the [He]/[H_2] mixing ratio. The uncertainty in temperature above 300 km is estimated to be ±10°K for the UVIS derivation (Shemansky and Liu 2009). The UVIS δ-Ori result is one of only two analyzed occultations from the sunlit atmosphere, the other being the Voyager 2 δ-Sco stellar ingress occultation (Vervack and Moses 2009). The ζ-Ori occultation results also show a distinct mesopause, but the mesopause temperature is warmer than that derived for the δ-Ori occultation, and the overall shape of the profile is more similar to that of the Voyager 2 δ-Sco egress occultation. The derived thermospheric temperature from

the ζ-Ori occultation is ∼407 K. These derived temperatures, plus the 460–500 K thermospheric temperature obtained from the six Voyager ultraviolet occultations from 1980 to 1981 (Vervack and Moses 2009) suggest temperature variability in Saturn's thermosphere as a function of location and/or time.

The above figures were all plotted as a function of altitude above the 1-bar pressure level, with an oblated spheroid model used to approximate the 1-bar pressure surface. Given that the radius of the 1-bar pressure level is not accurately known for Saturn (e.g., Lindal et al. 1985) and because planetary properties such as gravity vary strongly with latitude on this unusually shaped, extended-equatorial-bulge planet, such altitude or radius profiles do not provide a good, meaningful common scale for comparison of occultations from different latitudes. In fact, finding a good common scale for comparisons is problematic. Some investigators have tried to resolve this problem by converting their radial profiles obtained at a specific latitude to an "equivalent equatorial radius" by assuming an oblate-spheroid shape for the planet (e.g., Smith et al. 1983). However, Saturn's zonal winds, which are not uniform with latitude, perturb the planet's shape significantly such that an oblate spheroid is an unacceptable approximation that can introduce errors of more than 100 km in altitude. Converting to a pressure scale for direct comparisons would be ideal, but that method also introduces uncertainties. In Fig. 8.3 we plot the derived temperature and concentration profiles as a function of pressure from most ultraviolet occultations analyzed to date – the preliminary UVIS 2005 δ-Ori DOY 103 occultation (Shemansky and Liu 2009), the Earth-based 28 Sgr stellar occultations (Hubbard et al. 1997), the original Smith et al. (1983) Voyager 2 δ-Sco egress occultation analysis, and the Vervack and Moses (2009) reanalysis of all the Voyager UVS occultations.

To get the pressures shown in Fig. 8.3, the H_2-density-radius profiles obtained from the Voyager occultations have been integrated from the top down to infer the pressure at each radius (see Vervack and Moses 2009), whereas the pressures for the other profiles were determined from either the hydrostatic equilibrium forward models (Shemansky et al. 2009) or from the H_2 densities and temperatures assuming that H_2 is the main constituent and that the ideal gas law applies. This conversion from H_2 densities and temperatures to pressures is only reliable above the homopause level, where hydrocarbons and CH_4 have already diffused out, but not so high up that H begins to compete with H_2. Note from Fig. 8.3 the general consistency in the derived H_2 and H profiles for most of the occultations; most also merge smoothly with the Hubbard et al. (1997) ground-based stellar occultation H_2 density results. This consistency suggests that Saturn's thermospheric density structure is relatively uniform across latitudes (i.e., to within a factor of ∼2) on constant-pressure surfaces. On the linear temperature scale on the right-hand side of Fig. 8.3, differences between the different occultations are more apparent. The lower thermosphere of Saturn exhibits temperature variations of more than 100 K as a function of location or time. Even more striking is the much colder thermosphere derived from the Cassini UVIS results for the δ-Ori occultation in comparison with the other Voyager occultations, and that difference also shows up in the H_2 density profiles. As previously mentioned, the comparison of the Voyager and Cassini observations suggests latitudinal or temporal variations in thermospheric temperatures exist on

Fig. 8.3 The H_2 and H densities (*left*) and temperatures (*right*) as a function of pressure determined from the Cassini UVIS δ-Ori stellar occultation from 2005 at a dayside latitude of −42.7° (Shemansky and Liu 2009) are compared with various Voyager 2 UVS occultation retrievals (Vervack and Moses 2009) that have been smoothed to eliminate density scatter. The brown dot represents the Voyager 1 solar ingress occultation for which a full temperature profile could not be obtained
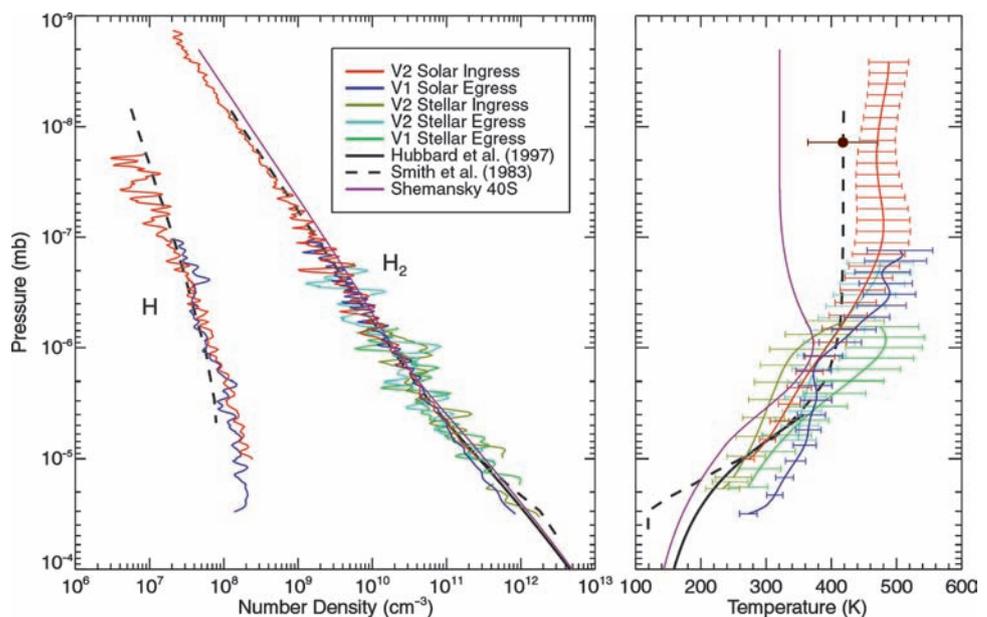
Saturn. Note, however, that the "wiggles" or "bulges" in the derived temperature profiles for several of the occultations should be interpreted with caution. If not dynamically supported, such structures would be smoothed out by conduction on very short time scales (see Section 8.4).

8.2.2 Determination of Atmospheric Properties from UVIS Spectra and Emission Maps

EUV/FUV spectra of the Saturn dayglow have been obtained with the Cassini UVIS. The UVIS spectra are the first observations of the excited atmosphere at solar minimum. The spectrum has been modeled in one dimension and pure hydrogen, constrained by ionospheric measurements (Nagy et al. 2006), and atmospheric structure, as a non-LTE system at the rotational level (Shemansky et al. 2009) with a purely solar-forced system. The model calculation establishes testable state populations, and all emission transitions in the system are predicted from radar frequencies to the EUV (Hallett et al. 2005a, b; Shemansky et al. 2009). Figure 8.4 shows an observed spectrum compared with the model calculation. The observed band intensities are a factor of 2.5 below those obtained at the Voyager encounter, and the spectra are qualitatively different, as is discussed by (Shemansky et al. 2009). Unlike the case for the Voyager observations (e.g., Shemansky and Ajello 2003), the Cassini UVIS dayglow spectra can be entirely explained (in terms of both spectral content and absolute brightness) by solar radiation deposition alone, with no excited electron source required (Shemansky et al. 2009). Note also that the non-LTE model calculations shown in Fig. 8.4 (Shemansky et al. 2009) predict a short-lived (∼3,000 s) plasma population dominated by H_3^+ below about 2,000 km,
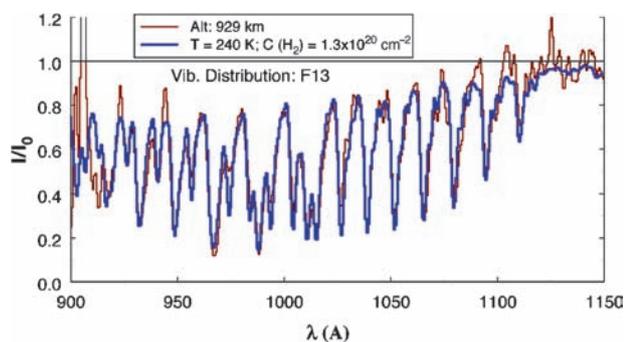
Fig. 8.4 UVIS EUV stellar occultation transmission spectrum obtained 2005 DOY 103 at an effective impact parameter of 929 km. The rotational temperature is iteratively determined assuming LTE. The vibrational population distribution is non-LTE, determined iteratively by fitting separate vibrational vectors into the model for optimal match to spectrum (Shemansky and Liu 2009)

rather than H^+, and that invoking H_2O to act as a quenching agent for H^+ – a process that has been introduced by several ionospheric modelers to help explain the observed electron-density profiles (see Section 8.6) – may not be necessary at these lower altitudes.

Cassini UVIS maps of the Saturn magnetosphere have revealed distinct atomic hydrogen distributions in the region inside 4 R_S of planet center, showing the gas escaping the top of the thermosphere (Shemansky et al. 2009). The observed H Lyα brightness of the peak emission is about 1,000 R. The measurements in the sunlit southern latitudes show atomic hydrogen escaping at all latitudes below the auroral regions. The anti-solar side of the planet shows an emission distribution consistent with a combination of an orbiting and ballistic hydrogen source in the subsolar thermosphere. The hydrogen atoms in this sub-orbital portion of the corona re-enter the thermosphere within about 5 hours. A larger more broadly distributed hydrogen corona fills the magnetosphere to beyond 45 R_S in the orbital plane. This distribution is asymmetric in local time and similar to an image obtained with Voyager 1 in a different observational geometry (Shemansky and Hall 1992). The escape of atomic hydrogen from the top of the atmosphere requires a translational energy ranging from 5.5 eV at the equator to 7.2 eV at the poles and thus provides an indication of the total energy needed to create these hydrogen atoms and in turn the energy deposited in the upper atmosphere. However, there are clear problems associated with this energy estimate. It is about ten times the solar input and it cannot come from particle precipitation, because of the upper limit set by H_2 optical emissions. Shemansky et al. (2009) suggest that the hot H is the result of a high temperature (∼20,000 K) electron population; this is within the constraints set by the observed H_2 UV emissions, but the basic source of this energy still remains to be identified.

8.3 Theoretical and Empirical Models of the Neutral Upper Atmosphere: Chemistry and Atmospheric Transport in the Homopause Region

Methane is photolyzed just below its homopause level, and the pressure at which photolysis occurs can affect the subsequent production and loss of complex hydrocarbons in Saturn's atmosphere (e.g., Moses et al. 2000). Therefore, the homopause-region observations and corresponding theoretical implications are discussed in some detail here, although a full discussion of hydrocarbon photochemistry is deferred to Chapter 5 by Fouchet et al. (2009) in this book. The variation of the methane abundance with altitude is controlled by molecular diffusion and/or transport – photolysis and subsequent photochemistry represent a much smaller

perturbation of the CH_4 concentration profile. The solar and stellar ultraviolet occultation results described in Section 8.2.1 therefore provide important information needed for inferring vertical transport properties in Saturn's atmosphere (e.g., Atreya et al. 1984).

One convenient means of parameterizing atmospheric mixing in one-dimensional atmospheric models has been the use of a vertical eddy diffusion coefficient K_{zz} (e.g., Atreya et al. 1984; West et al. 1986; Strobel 2005). Different investigators have derived different K_{zz} values from the same Voyager 2 UVS δ-Sco stellar egress occultation (cf. Festou and Atreya 1982; Smith et al. 1983), illustrating the possible complexities and model dependencies of occultation analyses. Moses et al. (2000) have demonstrated that much of the difference in the quoted K_{zz} values from these two investigations results from different assumptions about the shape of the K_{zz} profile rather than true differences in the derived radius level of the methane homopause on Saturn. Both Festou and Atreya (1982) and Smith et al. (1983) agree that atmospheric mixing is relatively vigorous on Saturn compared with Jupiter and the other giant planets (cf., Atreya et al. 1984; Yung and DeMore 1999; Moses et al. 2004, 2005) such that the methane homopause is located at a relatively high altitude on Saturn.

This Voyager result was contradicted in part by the recent Cassini observations described above. Figure 8.1 demonstrates that at the time (April, 2005) of the Cassini UVIS stellar occultation at −42.7° latitude (Shemansky and Liu 2009), the methane homopause was found to reside at a significantly lower altitude – and several pressure scale heights below – the homopause level determined for the Voyager 2 δ-Sco egress occultation (August, 1981) at 3.8° latitude (see Smith et al. 1983; Shemansky and Liu 2009; Vervack and Moses 2009). Although the altitude scales at the different latitudes differ significantly due to the unusual shape and gravity variation with latitude/altitude on this rapidly rotating and high-zonal wind planet, a real difference in homopause levels of the two occultation sites does exist when the methane profiles are compared in pressure or H_2-density space. A reanalysis of all the Voyager solar and stellar UVS occultations (Vervack and Moses 2009) confirms that the methane homopause pressure level varies significantly with latitude and/or time on Saturn due to latitudinal and/or temporal variations in eddy mixing or vertical winds. This variation is aptly demonstrated in Fig. 8.5, which shows that the implied methane homopause pressure level is a full two orders of magnitude different between the Voyager 2 solar ingress occultation results at 29.5° latitude (Vervack and Moses 2009; methane homopause located near 10^{-6} mbar) and the Cassini UVIS stellar occultation results at −42.7° latitude (Shemansky and Liu 2009; methane homopause located near 10^{-4} mbar).

By comparing photochemical model results with the concentration profiles derived from the occultations, certain chemical and dynamical properties of Saturn's atmosphere can be constrained. In Fig. 8.5, the Voyager 2 solar ingress occultation results at 29.5° latitude (Vervack and Moses 2009) and the Cassini UVIS stellar occultation results at −42.7° latitude (Shemansky and Liu 2009) are compared with three photochemical models. The green profile, which represents a model that fits the Voyager 2 solar ingress UVS occultation light curves at methane-sensitive wavelengths (Moses and Vervack 2006), uses the hydrocarbon photochemistry from "Model C" of Moses et al. (2005), and has strong eddy mixing, with $K_{zz} \sim 2 \times 10^8\,cm^2\,s^{-1}$ at $\sim 1 \times 10^{-5}$ mbar, dropping with decreasing altitude to $K_{zz} \sim 3 \times 10^7\,cm^2\,s^{-1}$ at $\sim 10^{-4}$ mbar, down to $K_{zz} \sim 1 \times 10^5\,cm^2\,s^{-1}$ at ~ 0.1 mbar. Although this model fits the methane concentration versus radius profile derived from the Vervack and Moses (2009) reanalysis of the Voyager 2 solar ingress UVS occultation quite well, the C_2H_2 and C_2H_4 model-data comparisons are much worse, suggesting problems with the chemistry and/or transport parameters in the models. The reaction rate coefficients adopted in the models are often not measured at the low pressures (and temperatures) typical of the homopause region of Saturn, and occultation observations such as these might be very useful for further constraining the chemistry and for identifying the key low-pressure reactions.

In order to fit the methane profile derived from the −42.7° Cassini UVIS δ-Ori occultation, eddy mixing must either be much less vigorous than for the Voyager case or downward winds must come into play. The red curve in Fig. 8.5 represents a model that also uses the "Model C" photochemistry of Moses et al. (2005) but has much weaker eddy mixing than the green curve described above, such that $K_{zz} \sim 2 \times 10^6\,cm^2\,s^{-1}$ at 1×10^{-4} mbar. Even with this low value of K_{zz}, the model overpredicts the CH_4 concentration near 10^{-3} mbar. One interesting point to note is that both occultation profiles shown in Fig. 8.5 have much "sharper" C_2H_2 profiles than the models: the models underpredict C_2H_2 mixing ratios at the level of the peak mixing ratio and overpredict the C_2H_2 mixing ratio at lower altitudes. This failure of the models remains to be explained, but may provide useful constraints on the chemistry. For example, the chemistry in "Model A" of Moses et al. (2005) provides sharper C_2H_2 profiles and may better represent the situation on Saturn (see Table 8.1 of Moses et al. 2005 for a discussion of the differences between the chemistry in Models A and C).

The blue curve in Fig. 8.5 represents a model that uses "Model A" chemistry (to better reproduce the "sharpness" in the C_2H_2 profiles), assumes $K_{zz} \sim 2 \times 10^6$ at 10^{-4} mbar, (varying with the inverse of the square root of the pressure between 0.5 and 2×10^{-4} mbar), and adds a
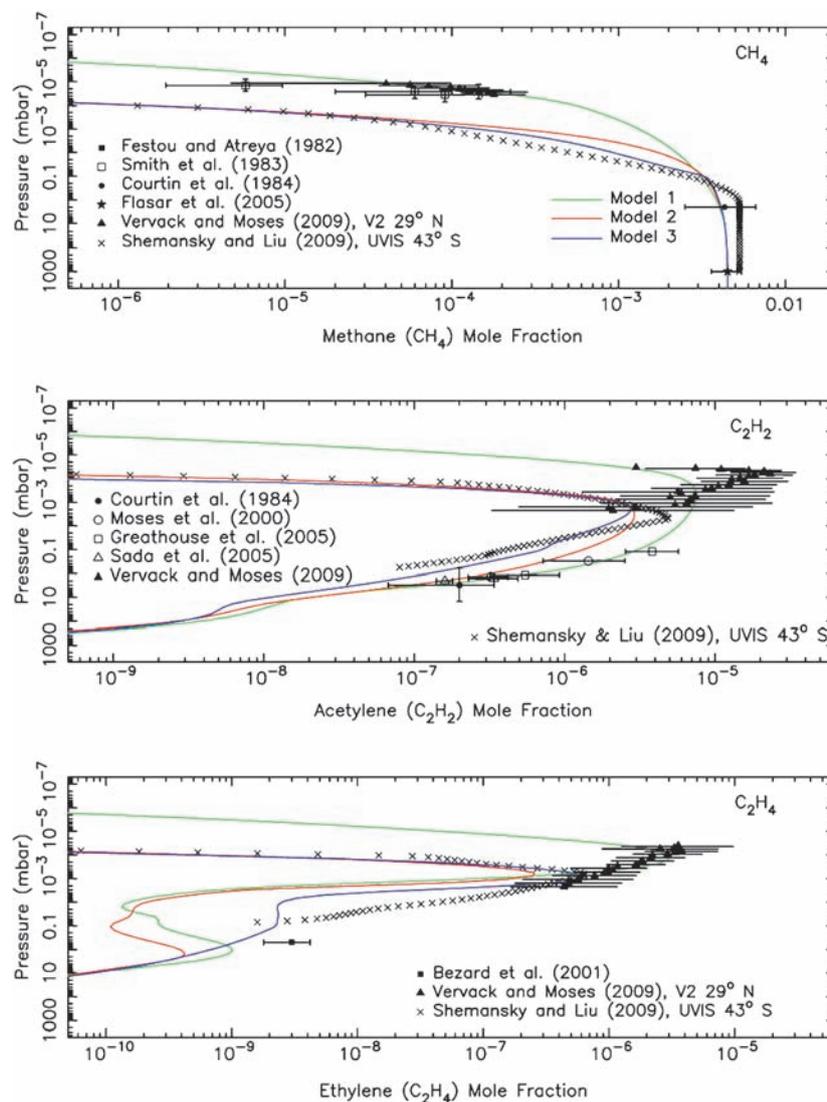
Fig. 8.5 Comparisons between photochemical models (colored solid lines) and the Voyager 2 UVS solar ingress occultation results (solid triangles, Vervack and Moses 2009), the Cassini UVIS δ-Ori −42.7° latitude stellar occultation results (×'s, Shemansky and Liu 2009), and various other infrared and ultraviolet data sets. The main point here is that the methane homopause was apparently located much higher in Saturn's atmosphere (i.e., at a pressure two orders of magnitude lower) at 29° latitude at the time of the Voyager 2 solar ingress occultation in 1981 than it was at −42.7° latitude at the time of the Cassini UVIS δ-Ori occultation in 2005, which indicates differences in vertical transport characteristics with latitude and/or time on Saturn. A secondary point is that current photochemical models do not accurately reproduce the vertical profiles derived for the C_2H_x hydrocarbons

downward wind of $-0.1\,\mathrm{mm\,s^{-1}}$ above 0.1 mbar to better fit the CH_4 profile from the Cassini UVIS stellar occultation (Shemansky and Liu 2009). Such vertical wind velocities are not unreasonable in the mesopause region (Müller-Wodarg et al. 2006) and would imply vertical transport time scales of order 10 years in the middle atmosphere. This model does a better job of reproducing the derived Cassini UVIS methane and acetylene profiles, but the fit is by no means perfect.

Given the overall variation in hydrocarbon profiles from the different Voyager UVS occultations (Vervack and Moses 2009) and the Cassini UVIS δ-Ori occultation (Shemansky and Liu 2009), it appears that the standard view of vigorous atmospheric mixing in Saturn's middle atmosphere is not valid for all latitudes and times. Vertical winds and/or atmospheric mixing appear to be highly variable on Saturn, and atmospheric dynamics may play the dominant role in controlling species abundances in the upper regions of Saturn's middle atmosphere. The time scales involved are comparable to the lifetime of the Cassini mission, and the numerous solar and stellar occultations acquired by Cassini UVIS to date, along with the future planned occultations, may be invaluable in constraining stratospheric circulation on Saturn.

Caution must be exercised in interpreting the ultraviolet occultations, however. The occultations provide reliable descriptions of the concentration variations as a function of radius, albeit with some embedded assumptions about ultraviolet absorption cross sections, spectral behavior, spatial homogeneities and appropriate data processing procedures built into the analyses. Given uncertainties in Saturn's 1-bar radius as a function of latitude, in Saturn's temperature profile in the entire region from 1 bar to the high-altitude occultation levels, in Saturn's mean molecular mass variation with altitude, and in Saturn's zonal wind variation with altitude, any attempts to convert concentration-radius profiles to concentration-altitude profiles (as in Fig. 8.1 above), concentration-pressure profiles (as in Figs. 8.3 and 8.5 above), or any other such scenarios will necessarily require hydrostatic equilibrium solutions that will be highly model dependent. Similarly, during the occultation, the transmission from the H_2-sensitive wavelengths drops to zero by the radius level at which CH_4 absorption starts to be significant, which can complicate derivations of the mixing ratio (as opposed to concentration) profiles as a function of radius. All these complications and model dependencies can explain some of the very different results that have been obtained from different analyses of the same occultation data sets (e.g., Yelle et al. 1996 vs. Festou et al. 1981 for Jupiter, Festou and Atreya 1982 vs. Smith et al. 1983 for Saturn). Near-simultaneous observations that record temperature structure in the upper troposphere and middle atmosphere (e.g., from Cassini CIRS) in the regions probed by the ultraviolet occultations will greatly aid the occultation analyses. Analyses of the UVIS solar occultations, which unlike stellar occultations contain a signature atmospheric absorption in the H_2 continuum below 91.2 nm, will also be very helpful in defining thermospheric temperatures on Saturn.

8.4 Theoretical and Empirical Models of the Upper Atmosphere: Temperature Structure, Energy Balance, and Dynamics

8.4.1 Thermal Structure

The two Voyager radio occultation observations provided temperature values for the troposphere and stratosphere (Lindal et al. 1985; Lindal 1992). No information about the mesosphere could be inferred from the Voyager data, but results from ground based observations of the stellar occultation of 28 Sgr in 1986 suggested virtually constant temperatures there with a value of 141 K between 1 mbar and 0.3 μbar (Hubbard et al. 1997). Their measurements also extended into the lower thermosphere, near 0.05 μbar.

Thermospheric temperatures could first be inferred from the Voyager solar and stellar occultation experiments with the ultraviolet spectrometer (UVS) (Festou and Atreya 1982; Smith et al. 1983). These measurements placed the base of Saturn's thermosphere near the 0.1 μbar level. Initially, non-auroral exospheric temperatures on Saturn were a subject of debate since two very different values were derived from the Voyager data. The solar occultation experiment obtained a value of 420 ± 30 K near 30°N latitude (Smith et al. 1983) while the stellar occultation experiment yielded a value of 800 (+150/–120) K near 4°N latitude (Festou and Atreya 1982). These differences are not the result of the different occultation approaches and such extreme differences are not likely to be present in the atmosphere at such small latitudinal distances; the 30°N occultation result is now generally accepted as being more realistic (e.g., Vervack and Moses 2009). A comprehensive discussion of these two measurements was presented by Smith and Hunten (1990). Recently, the Voyager UVS data have been reanalyzed by Vervack and Moses (2009) and Shemansky and Liu (2009) and are shown in Figs. 8.2 and 8.3 alongside the recent Cassini UVIS occultation data discussed above (Shemansky and Liu 2009).

The thermal profile of Saturn' thermosphere, as those of the other gas giants, is poorly understood (Strobel and Smith 1973; Yelle and Miller 2004). As shown recently by the calculations of Müller-Wodarg et al. (2006) with the Saturn Thermosphere Ionosphere General Circulation Model (STIM), solar EUV heating produces exospheric temperatures on Saturn ranging from 153 K at solar minimum to 160 K at solar maximum. Those simulations assumed heating efficiencies of 50%, but even increasing this value to an unrealistic 100% raised solar driven exospheric temperatures only by 13 K (25 K) at solar minimum (maximum). It is therefore energetically not possible to heat Saturn's upper atmosphere with solar EUV radiation alone to the observed temperatures. These simple experiments also showed the solar cycle variability of exospheric temperature expected from solar EUV heating alone to be in the order of tens of degrees or less.

The main constraints on Saturn's upper atmosphere from ground-based observations have been obtained with measurements of H_3^+ emissions. The initial detection of these emissions from Saturn was made by Geballe et al. (1993) in 1992, using the CGS4 spectrometer on the United Kingdom InfraRed Telescope (UKIRT Mauna Kea, Hawaii). They found that spectra at the northern and southern limbs had roughly the same intensities, and that they were not able to measure H_3^+ emission at the equator. However, their initial measurements indicated that, for Saturn, the line intensity fell off more slowly from the limbs to the equator than was the case for Jupiter, for which auroral emission had been first detected in 1988 (Drossart et al. 1989). This indicated that the morphology was somewhat intermediate between

Jupiter, with its emission strongly concentrated around the auroral/polar regions (Baron et al. 1991), and Uranus, for which a planetwide H_3^+ glow seemed more likely (Trafton et al. 1993). Geballe et al. (1993) determined the best-fit temperature for their polar spectra on Saturn to be around 800 K, lower than for Jupiter, for which temperatures between 900 K and 1,100 K were found in the auroral regions (Drossart et al. 1989; Lam et al. 1997), and the column density of H_3^+ on Saturn to be around 1.0×10^{15} m^{-2}, about 10–50 times less than for Jupiter's auroral zones. The auroral temperature value derived by Geballe et al. (1993) is around twice the equatorial value proposed by Smith et al. (1983). Stallard et al. (1999) calculated that the total H_3^+ emission from Saturn might be as high as $1.5 \pm 0.3 \times 10^{11}$ Watts, if the temperature ($\sim$800 K) derived by Geballe et al. (1993) was correct. This figure was $\sim$50 times less than the Jovian H_3^+ emission, but still high compared with UV emission from Saturn.

The first challenge to the "high" temperature for Saturn's auroral exosphere came from Miller et al. (2000), whose analysis of later (1999) UKIRT data indicated that 600 K was more likely, but this, too, was in error. It is now clear that the best fit temperature for Saturn's upper atmosphere, at the level of the peak H_3^+ emission in the auroral/polar zones is much closer to 400 K than 800 K. Melin et al. (2007) reanalysed the UKIRT spectra taken in 1999, and others obtained in 2004 and 2005. They found a best-fit temperature of 380 ± 70 K for the 1999 data, and 420 ± 70 K for 2004. Averaging gave 400 ± 50 K for the best fit Saturn polar thermospheric temperature. What emerged clearly was the variability in the ion column densities – assuming a constant temperature of 400 K gave 2.1×10^{16} m^{-2} and 2.9×10^{16} m^{-2} for the 1999 and 2005 data, respectively, but 20.0×10^{16} m^{-2} for 2004. The implications for the energy balance in Saturn's upper atmosphere of this large variation in H_3^+ column density are discussed below.

8.4.2 Energy Balance and Dynamics

Over the past few years, there has been considerable progress in understanding the upper atmosphere energetics and dynamics of Saturn's polar regions as a result of H_3^+ observations and modeling. Based on HST UV images, Cowley et al. (2004) first proposed that the main auroral oval resulted from the interaction between the solar wind and Saturn's magnetosphere, and, although other mechanisms have not been entirely ruled out, this seems to be a promising proposal. The Cowley et al. (2004) model of plasma dynamics in the ionosphere included flows from the Dungey (1961) and Vasyliunas (1983) cycles, and a general lag to corotation with the planet across the entire auroral/polar region due

to interactions with the solar wind, a mechanism first put forward by Isbell et al. (1984). Measurements of the Doppler shifting of the H_3^+ emission line at 3.953 mm generally supported the picture of a general lag to corotation across the polar regions (Stallard et al. 2004). Cowley et al. (2004) derived a value for the angular velocity of the auroral/polar ionosphere of $\Omega_{ion} = 0.24\,\Omega_{Saturn}$, assuming a solar wind velocity of 500 km/s and an effective ionospheric Pedersen conductivity of 0.5 mho. Stallard et al. (2004) measured a value of $\Omega_{ion}/\Omega_{Saturn} = 0.34$, which suggested a value for the effective (height-integrated) Pedersen conductivity of the ionosphere of $\Sigma_P^* = 0.82$ mho, if the solar wind velocity remained at 500 km/s.

The consequences of this lag to corotation for energy balance in the Saturnian polar upper atmosphere are considerable. The auroral/polar ionosphere is produced mainly by charged particle precipitation. On Jupiter, particle precipitation may deposit in the order of 10^{12} Watts planetwide, but this energy input is largely balanced by emission from H_3^+ (Miller et al. 1994, 2006) – the so-called H_3^+ thermostat ($\sim$50–80%). Much more energetically important, however, is the energy generated by Joule heating, resulting from equatorward currents across the auroral oval, and the westward winds produced by Hall drift (see Smith et al. 2005; Miller et al. 2006). On Saturn, Melin et al. (2007) have shown that the H_3^+ thermostat is much less effective ($\sim$1%) than it is for Jupiter (Melin et al. 2006) (and probably for Uranus). Particle precipitation into the auroral/polar regions is thought to deposit around 10^{11}W, but Joule heating (ion drag) is thought to be a factor of 10 larger (Cowley et al. 2004; Miller et al. 2006).

In an attempt to understand the role of magnetospheric energy input globally, Müller-Wodarg et al. (2006) and Smith et al. (2005) carried out simulations in which Joule heating was applied at polar latitudes, depositing 8.8 TW in Saturn's lower polar thermosphere, a factor of 35–65 more than provided by planet-wide solar EUV heating. Their calculations did not include H_3^+ cooling, so polar temperatures reached around 1,000 K. Despite these unrealistically high values, equatorial temperatures in their calculations did not exceed around 250 K, considerably lower values than observed. In these simulations Saturn's fast rotation via Coriolis accelerations generated a primarily zonal flow in the atmosphere, which in turn prevented meridional transport of energy from pole to equator. In fact, calculations by Smith et al. (2007), which included the effects of ion drag that generates westward flows, suggested that polar heating on Saturn could lead to slight cooling of the low latitude thermosphere via adiabatic cooling. These calculations have assumed steady-state conditions and the effects of highly (short-term) variable inputs into Saturn's auroral/polar regions witnessed in the VIMS images (Stallard et al. 2008) on the horizontal distribution of magnetospheric energy have

yet to be examined. Furthermore, future studies need to calculate the magnetosphere-ionosphere-thermosphere coupling self-consistently to allow two-way coupling between these systems, an aspect that will critically affect the effective Pedersen conductivity. Despite these shortcomings of the calculations, they have illustrated the sensitivity of the energy distribution in Saturn's thermosphere to global circulation via energy redistribution processes such as advection and adiabatic heating and cooling. The dynamics of Saturn's thermosphere are as yet unconstrained except for measured ion velocities in the auroral regions, and it should be mentioned that the calculations by Müller-Wodarg et al. (2006) and Smith et al. (2005) ignored effects of ion drag.

To "fill in" the low latitude "energy hole" and obtain thermospheric temperatures consistent with observations, Müller-Wodarg et al. (2006) proposed the presence of an additional unidentified energy source at low latitudes, an aspect we explore further in this section. Figure 8.6 shows thermospheric temperatures as derived from the Voyager 2 UVS solar ingress and stellar egress occultations by Smith et al. (1983) and from the reanalyzed UVS solar ingress occultation by Vervack and Moses (2009) (blue symbols). Also shown (light blue curve) are temperatures from the Cassini UVIS δ-Ori occultation presented in this chapter (Fig. 8.2). Super-imposed in Fig. 8.6 (red lines) are zonally averaged temperatures from three simulations carried out

with the STIM General Circulation Model of Müller-Wodarg et al. (2006) for different empirical energy sources. Simulations A and C considered heating near the exobase and mesopause, respectively, and simulation B represents an in-between case. In Simulation A 3.8 TW is deposited planet-wide, with the volume heating rate peaking at the 7.3×10^{-10} mbar level, having a Gaussian shape with a mean half width of 2.5 scale heights. In Simulation B 5.2 TW is centered at the 2×10^{-7} mbar level and in Simulation C the volume heating rate peaks at the lower boundary pressure (1.6×10^{-5} mbar) with a total energy of 15 TW. As expected, the energy necessary to reach the desired exospheric temperatures becomes smaller when deposited higher up in the thermosphere since molecular conduction, a key energy loss process, becomes less effective at lower densities in the atmosphere. The profiles in Fig. 8.6 are for a mid-latitude location of 30°N consistent with the location of the Voyager 2 UVS solar ingress observations. While the observations by Cassini UVIS were made at 42.7°S and 15.2N, little difference was found in the simulations between these locations.

A key difference between the three simulations presented in Fig. 8.6 is the slope of the lower thermosphere temperature which is crucially affected by the altitude/pressure of peak volume heating deposition. Both the Voyager and Cassini derived temperature profiles are best fit by simulations B and C, where energy is deposited near and below the 10^{-7} mbar level, whereas heating in the exosphere (Simulation A) produces a temperature shape that is less consistent with these observations. It should be noted, though, as described in Section 8.2.2, that recent Cassini UVIS observations of atomic hydrogen escape have suggested the possibility of significant energy deposition at the top of the thermosphere, consistent with Simulation A, a topic which needs further investigation beyond the scope of this chapter. Depending on the exact altitude of energy deposition, the calculations suggest a total additional energy of between 5 and 13 TW being necessary to raise thermospheric temperatures at low latitudes to the observed levels. Locally, the height integrated heating rates which were applied in simulations B and C are 0.08 and 0.30 mW/m^2, respectively. The model cannot currently reproduce and explain the negative temperature gradient observed by the Cassini UVIS stellar occultation curve at $-42.7°$ above the 1×10^{-6} mbar level. While the response of the thermosphere to three possible cases of heating functions was examined, no attempt was made to explain the origin of this empirical heating, if it exists in reality. The heating function of Simulation C may suggest energy propagating upward from below, possibly via waves, but at present there are too few constraints to characterize the waves in Saturn's upper atmosphere. The required energy may also result from energy redistribution by global dynamics other than those simulated by Müller-Wodarg et al. (2006) and Smith et al. (2005).

Fig. 8.6 Temperatures in Saturn's upper atmosphere as inferred from observations of the Voyager 2 solar ingress (29°N) and stellar egress (4°N) occultations (*blue curve*) by Smith et al. (1983) and from a re-analysis of the Voyager 2 UVS solar ingress occultation at 29°N (blue symbols) by Moses and Vervack (2006). Also shown are temperatures inferred from Cassini UVIS observations in 2005 (*light blue curve*) near 42.7°S (Shemansky and Liu 2009). Red lines denote temperatures at 30°N from calculations with the model by Müller-Wodarg et al. (2006), assuming three different forms of empirical heating functions. Simulation A (dashed) assumes 3.8 TW deposited near the 7.3×10^{-10} mbar level, Simulation B (solid) assumes 5.2 TW deposited near the 2×10^{-7} mbar level and Simulation C (dashed-triple-dotted) assumes 15 TW deposited near 1.6×10^{-5} mbar

Fig. 8.7 Terms of the energy equation in Simulation *B* of Fig. 8.6, extracted at 30°N. The empirical heating source is balanced primarily by vertical molecular conduction. Vertical winds play an important role in depositing energy at those latitudes via advection and adiabatic heating

To analyze in more detail the energy balance in these simulations, Fig. 8.7 shows zonally averaged volume heating and cooling rates from simulation *B* at 30°N. Apart from the imposed empirical heating function, the main energy sources at mid latitudes are adiabatic heating and vertical advection. The combined energy sources are balanced by cooling from vertical molecular conduction. While other processes such as solar EUV heating and horizontal advection are included in the calculations, their importance is negligible compared with the above heating and cooling processes. The figure illustrates the importance of dynamical terms for the energy balance in Saturn's thermosphere, emphasizing the need to study Saturn's energetics with global dynamical models. Polar Joule heating generates strong upwelling poleward of around 60° with vertical velocities of possibly several meters per second (Müller-Wodarg et al. 2006). The high latitude heating generates a global circulation cell that leads to downwelling equatorward of around 50° with vertical velocities of up to around 1 m/s. This downwelling leads to adiabatic heating and downward transport of energy from above, where the thermosphere is hotter. While Fig. 8.7 refers to one particular case of empirical heating, namely simulation *B*, the same energy redistribution processes are important in the other heating cases we calculated.

8.5 Observations of the Ionosphere

8.5.1 Radio Occultation Observations of Electron Densities

Virtually all the observational evidence on the structure of the ionospheres of outer planets and their satellites has been obtained by the method of radio occultation (Lindal 1992;

Kliore et al. 2004). This technique yields the vertical structure of the total electron density, $N_e(h)$, from which the plasma scale height can be derived, but neither the plasma temperature nor the ion composition is directly revealed. Pioneer 11 and the two Voyagers provided the first six $N_e(h)$ profiles at Saturn (e.g., Atreya et al. 1984), and the initial phase of the Cassini mission yielded twelve near equatorial profiles (Nagy et al. 2006). More recently, as Cassini moved away from an equatorial orbit, mid and high latitude density profiles have also been obtained (Kliore et al. 2009). The average low, middle and high latitude density profiles from Cassini radio occultations are shown in Fig. 8.8a. An increase in the averaged electron densities with latitude is clearly visible in this figure and is discussed in Section 8.6. A decrease in the mean peak density and increase in the corresponding height from dusk to dawn was seen in the average low-latitude observations, consistent with the presence of molecular ions at lower altitudes, which decay rapidly at sunset. Thus, this preferential decrease at lower altitudes leads to a decrease in the peak density and an increase in the altitude of the peak during the night. No such dusk to dawn changes could be ascertained in the mid-latitude data. (Dawn and dusk do not have the same meaning at high-latitude). Significant variations were seen in the Cassini observations, which could not be attributed to latitude and/or local time changes. A possible explanation for this variability is changing chemistry rates (e.g., water inflow that can hasten recombination, Moore and Mendillo 2007), dynamics (e.g., gravity-wave interaction with the plasma, Matcheva et al. 2001), electrodynamic effects, or variability driven by changing ionizing particle influxes. Given the uncertainty in the topside ion composition, a great deal of uncertainty is associated in deducing the topside plasma temperature from the measured scale heights. Using some simplifying assumptions, the low-latitude scale heights lead to estimated temperatures in the range of about 600–800°K, but it is important to remember that very large uncertainties are associated with these values.

Figure 8.8b also shows the electron densities deduced from the S44 orbit entry occultation, which has a very sharp "bite-out" around 2,500 km, possibly the result of some wave activity (Matcheva et al. 2001) or a surge of water influx as discussed in Section 8.6.

8.5.2 Electron Density Variations Inferred from SEDs

Impulsive short-duration bursts of broadband radio emissions were detected by the planetary radio astronomy experiment aboard both Voyagers for a few days on either side of their closest approaches to Saturn (e.g., Warwick
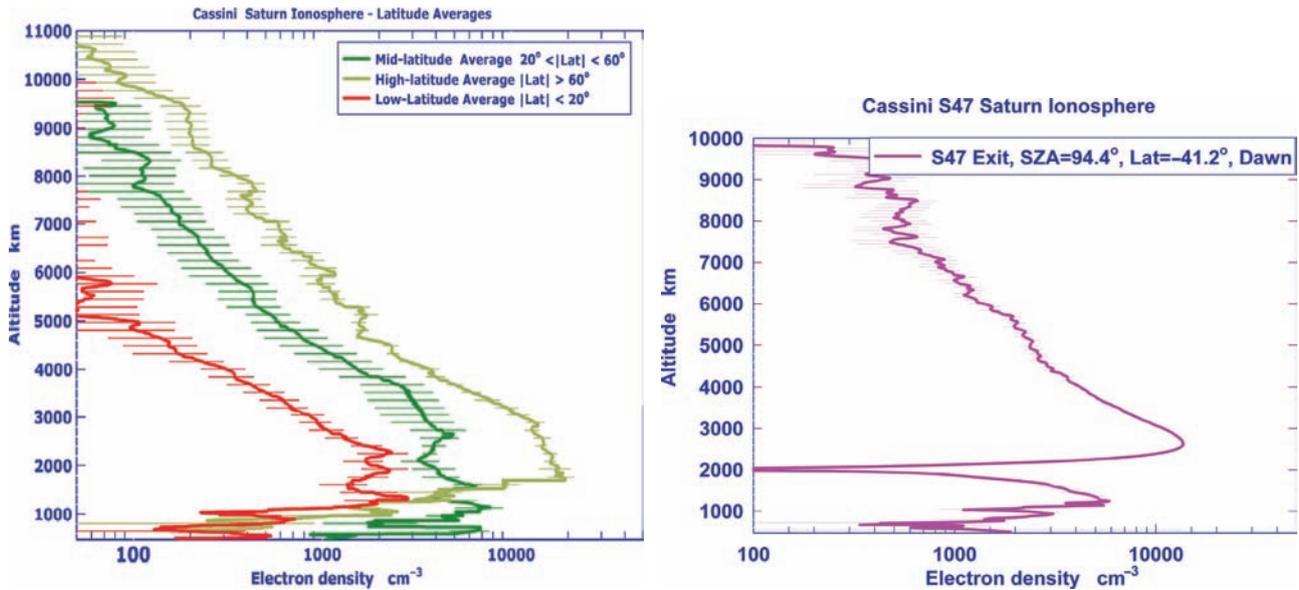
Fig. 8.8 (**a**) Averaged near-equatorial dusk and dawn electron density profiles (Nagy et al. 2006). (**b**) Electron density profile from the S47 exit observations showing a severe density "bite-out" (Kliore et al. 2009)
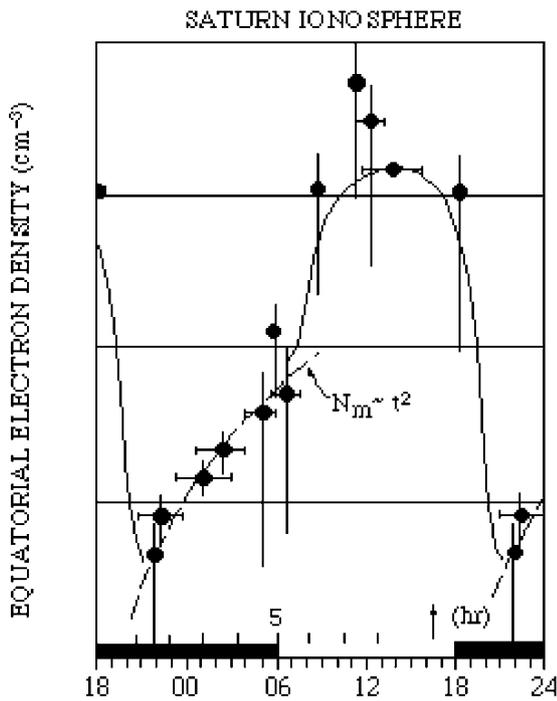
Fig. 8.9 SED inferred electron densities at Saturn from Kaiser et al. (1984)

et al. 1982). Dubbed Saturn Electrostatic Discharges (SEDs), they are now thought to be the result of low-altitude lightning storms. While there was some initial controversy over whether SEDs originated in Saturn's rings or atmosphere, Kaiser et al. (1983) demonstrated clearly that an atmospheric source was more likely. As final confirmation, Cassini's

Imaging Science Subsystem instrument has imaged bright clouds whose periods matched contemporaneous SED storm detections. Four such correlated visible and radio storms have been observed as of March 2007 (Dyudina et al. 2007).

SED emission from a lower atmospheric discharge source would have to pass through Saturn's ionosphere in order to be observed by a spacecraft, and therefore the lower frequency cutoff of the emission could contain information regarding the plasma frequency of the intervening plasma. Kaiser et al. (1984) estimated the local time dependence of Saturn ionospheric density based on the low frequency SED cutoffs observed. Their results are presented in Fig. 8.9, which implies a diurnal variation in electron density of two orders of magnitude – from $10^3\,\mathrm{cm}^{-3}$ at midnight to $10^5\,\mathrm{cm}^{-3}$ at noon. The SED-inferred electron densities at dawn and dusk were of order $10^4\,\mathrm{cm}^{-3}$, in agreement with the Voyager radio occultation data (Atreya et al. 1984). Thus far the observations of SEDs by Cassini have been highly sporadic, in contrast to the near constant occurrence during Voyager fly-bys, yet the inferred electron densities reproduce essentially the same diurnal behavior (Fischer et al. 2008 and references therein).

8.5.3 Ground Based Observations of H_3^+ Emission

Observations of optical signatures of ionospheric plasma at Saturn present a considerable challenge. The terrestrial detection of H_3^+ from Saturn, at infrared wavelengths, was discussed in Section 8.4.1. These observations found roughly

the same brightness at the northern and southern limbs, with no detections achieved at middle and equatorial latitudes. This argued clearly for an auroral source of the emission, and hence of high-latitude ionospheric plasma produced by incoming magnetospheric charged particles that far exceeded ionization produced by sunlight. As with the radio occultation and SED results, the dominant message from the H_3^+ observations is one of extreme variability. For example, Melin et al. (2007) analyzed the spectra taken in 1999, 2004 and 2005 at the United Kingdom InfraRed Telescope (UKIRT) on Mauna Kea, Hawaii UKIRT and found that the column contents varied considerably, ranging from ~ 2 to $\sim 20 \times 10^{16}\,\mathrm{m}^{-2}$. These are high values of H_3^+ column content for a giant planet's ionosphere, with the upper value comparable to the TEC levels measured at Earth. For comparison, with solar flux being the only ionizing source considered, model calculations by Moore et al. (2004) predicted the auroral H_3^+ column content to be $\sim 0.5 \times 10^{16}\,\mathrm{m}^{-2}$ and the TEC in the summer hemisphere to be $\sim 2 \times 10^{16}\,\mathrm{m}^{-2}$. As noted in Fig. 8.8b, Cassini electron density values are higher at high latitudes in comparison to the equator, and thus Saturn's ionosphere is likely the result of a blend of photo-production and auroral-production of a hydrogen plasma system, which provides a significant challenge to understand.

8.6 Models of Ionospheric Structure, Composition and Temperatures

8.6.1 Background Theory and Early Models

The first theoretical attempt at modeling Saturn's ionosphere came from McElroy's (1973) review of the four giant planets' ionospheres. He outlined most of the important photochemical reactions that all future work would draw from, and highlighted some issues that remain relevant today. The major reactions, which were usually considered, are as follows (for the sake of brevity only photoionization/photodissociation is indicated, but the same processes can result from electron impact):

$$H_2 + h\nu \rightarrow H_2^+ + e \tag{8.1a}$$

$$\rightarrow H^+ + H + e \tag{8.1b}$$

$$\rightarrow H + H \tag{8.1c}$$

$$H + h\nu \rightarrow H^+ + e \tag{8.2}$$

$$H_2^+ + H_2 \rightarrow H_3^+ + H \tag{8.3}$$

$$H_3^+ + e \rightarrow H_2 X^1\Sigma_g^+ (v : J) + H^* \tag{8.4a}$$

$$\rightarrow H^* + H^* + H^* \tag{8.4b}$$
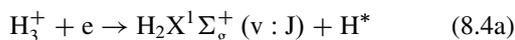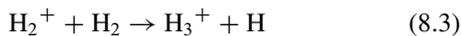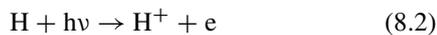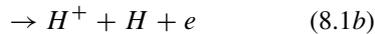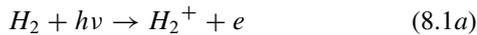
Reactions between ions and hydrocarbons (e.g., CH_4) were predicted to result in a pronounced shoulder on the bottomside ionosphere (Atreya and Donahue 1975). Galactic cosmic-ray induced ionization in Saturn's ionosphere was also evaluated, finding that it is likely to lead to the creation of a low-lying ledge of plasma of $\sim 7{,}000\,\mathrm{cm}^{-3}$ at ~ 0.5 bar (Capone et al. 1977).

Radio occultation measurements of Saturn's electron density by Pioneer 11, Voyager 1 and Voyager 2 found an ionosphere of roughly $10^4\,\mathrm{cm}^{-3}$, an order of magnitude smaller than early theoretical predictions. Therefore, a mechanism for reducing the modeled electron density was required. The chemical loss included for H^+ in early models was radiative recombination, a very slow process. In order to reduce the modeled electron density two processes were suggested (McElroy 1973; Connerney and Waite 1984), both of which act by converting long-lived atomic H^+ ions into short-lived molecular ions. The first process is the charge exchange reaction between H^+ and vibrationally excited H_2 in its ground state, as indicated by Eq. (8.5).

$$H^+ + H_2\,(v \geq 4) \rightarrow H_2^+ + H \tag{8.5}$$
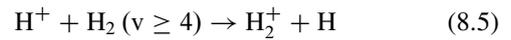
The main sources of vibrationally excited H_2 are via collisions with electrons (Hallett et al. 2005a):

$$e + H_2 X^1\Sigma_g^+\,(v_i : J_i) \leftrightarrow e + H_2 X^1\Sigma_g^+\,(v_j : J_j) \tag{8.6}$$
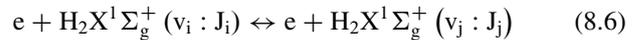
and H_3^+ recombination (Eq. 8.4a), while quenching of the excited H_2 can take place via collisions with electrons, both thermal and more energetic photoelectrons, H, H_2 and H^+. The rates for reaction (8.5) were not known for a long time and early attempts of estimating the vibrational population carried numerous uncertainties (Cravens 1987; Majeed et al. 1991). The reaction rate for (8.5) was established by Ichihara et al. (2000), and Shemansky and co-workers (e.g., Hallett et al. 2005a; Shemansky and Liu 2009) carried out comprehensive model calculations of the hydrogen system, as discussed later in this section.

The second suggestion (e.g., Connerney and Waite 1984) was that water introduced into the atmosphere from the rings and/or icy moons can reduce the H^+ density via a multistep process which converts it to H_3O^+, as shown below in Eqs. (8.7–8.9).

$$H^+ + H_2O \rightarrow H_2O^+ + H \tag{8.7}$$

$$H_2O^+ + H_2 \rightarrow H_3O^+ + H \tag{8.8}$$

$$H_2O^+ + H_2O \rightarrow H_3O^+ + OH \tag{8.9}$$

$$H_3O^+ + e \rightarrow H_2O + H \tag{8.10}$$
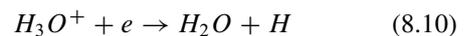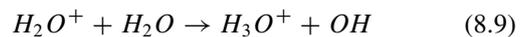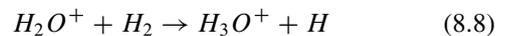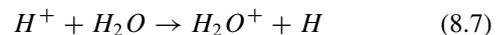
A discrepancy between the modeled and observed electron density had also arisen in the case of Jupiter earlier (Atreya

et al. 1979). In the Jovian case, modelers had invoked a distribution of vibrationally excited H_2 (see Eq. 8.5) elevated above LTE, along with postulated vertical plasma drifts, in order to reproduce Jovian electron density measurements (e.g., McConnell et al. 1982; Majeed and McConnell 1991). Still, as evidenced by the model results of Waite et al. (1983) that incorporated calculations of H_2 vibrational levels, the disagreement was more severe for Saturn. The determination of the vibrational distribution of H_2 remains an important topic today at both Jupiter and Saturn, as reviewed by Yelle and Miller (2004), and most recently outlined by Shemansky et al. (2009).

8.6.2 Modern Theory and Time Dependent Models

Due to Sun–Saturn–Earth geometry, radio occultations of Saturn all occur very near the dawn or dusk terminator –a period of rapid change for any solar produced ionospheric plasma (e.g., Schunk and Nagy 2009). While all previous modeling had been steady state, the large calculated electron densities and the dominance of H^+ over other ion species – whose chemical lifetime is large relative to a 10-h Saturn day – meant that little diurnal variation in electron density would be expected. Thus, the disagreement between steady-state models of Saturn's ionosphere and the spacecraft observations was the first indication that a time-dependent solution was required. In addition to the peak electron density discrepancy, the observations of Saturn Electrostatic Discharges (SEDs) implied a noon-to-midnight diurnal variation in electron density of two orders of magnitude, as indicated in Section 8.5.2 (Kaiser et al. 1984).

The first time-dependent solution to Saturn's ionosphere was a 1D chemical diffusive model that attempted to directly address the SED-inferred diurnal variation in electron density (Majeed and McConnell 1996). In order to reduce the implied noontime density of $10^5\,cm^{-3}$, and also to induce more dramatic diurnal variation, Majeed and McConnell (1996) tested a wide range of H_2 vibrational temperature profiles and topside H_2O influxes. However, despite being able to find combinations of the above two parameters that yielded good matches to radio occultation measurements, Majeed and McConnell (1996) could not reproduce the two orders of magnitude variation in electron density inferred from SEDs. Their strongest calculated noon-to-midnight variation was ∼7, though model simulations that yielded this strong diurnal variation were not able to simultaneously reproduce Voyager electron density altitude profile observations.

The next time-dependent ionospheric model developed for Saturn (Moses and Bass 2000) combined new Saturn observations (e.g., Feuchtgruber et al. 1997; Hubbard et al. 1997; Moses et al. 2000) and new reaction rates to derive a more accurate neutral atmosphere (e.g., Moses et al. 2000). Moses and Bass (2000) solved the coupled 1D continuity equations as a function of time for a comprehensive set of 63 neutral and 46 ionized species in Saturn's atmosphere. They addressed the ionospheric effects at Saturn for water, oxygen and magnesium influx, neutral winds, electric fields, and interplanetary dust. While Moses and Bass (2000) did not comment on the issue of SED-inferred diurnal variations in electron density directly, their standard model calculations utilized an empirically derived population of vibrationally excited H_2 along with a planet-wide water influx of $1.5 \times 10^6\,cm^{-2}\,s^{-1}$, and like the models of Majeed and McConnell (1996), Moses and Bass could not reproduce the large diurnal variations in electron density inferred from SEDs. The new global-average value of water influx, constrained by ISO observations and model calculations, was smaller than previously adopted values for Saturn (e.g., Connerney and Waite 1984). However, the planetary-averaged ISO observations could not explicitly exclude the possibility of strong latitudinal variations in water influx (e.g., Connerney 1986).

A recent model developed for Saturn's ionosphere is the Saturn-Thermosphere-Ionosphere-Model (STIM) (Müller-Wodarg et al. 2006). Whereas Moses and Bass (2000) provided a thorough analysis of Saturn's entire ionosphere with a focus on the lower hydrocarbon and metallic layers, STIM has concentrated on the major ions in the upper ionosphere, where the N_e peak lies. STIM is a global circulation model of Saturn's upper atmosphere (see Section 8.4), yet during its development, a series of 1D ionospheric studies were performed using the 3D thermosphere as a background. First, Moore et al. (2004) used a 1D time-dependent model that considered chemistry and plasma diffusion to investigate global ionospheric behavior, regimes of photochemical equilibrium within Saturn's ionosphere, ionospheric response to a wide range of water influxes and H_2 vibrational temperatures, and ionospheric conductivities (see Fig. 8.10a). Moore et al. (2004) extended the Majeed and McConnell (1996) parameter space results by demonstrating that no matter what combination of production and loss processes were included, chemistry alone could not reproduce a two order of magnitude diurnal variation in N_e during the short Saturn day. In addition, they modeled the ionospheric effects resulting from the pattern of shadows cast by Saturn's rings, finding sharp gradients and strong reductions in electron density. Mendillo et al. (2005) studied the seasonal variability of the patterns induced by ring shadowing in more detail. They argued that the electron density troughs produced by ring shadows (equinox for Voyager, solstice for Cassini) may lead to ionospheric "windows" through which SEDs could more easily escape, an interpretation that raises questions
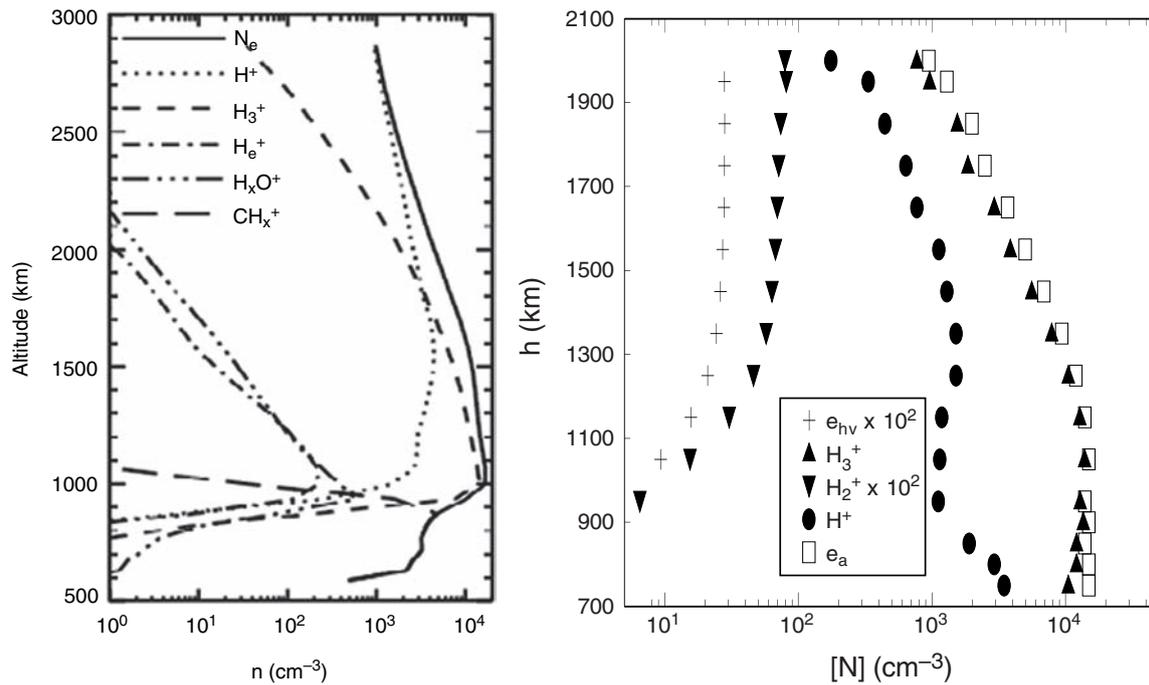
Fig. 8.10 (**a**) Noon ion density profiles from Moore et al. (2004). (**b**) Ion density profiles from Shemansky and Liu (2009)

regarding the use of SED detections as a type of ionospheric sounder for peak N_e. Second, Moore and Mendillo (2005) extended the STIM ionosphere into Saturn's inner plasmasphere based on Liousville's theorem and the method of Pierrard and Lemaire (1996, 1998), predicting an electron density of order $100\,\text{cm}^{-3}$ for Cassini's closest approach ($\sim 1.3R_S$), within the domain of extrapolation of the pre-SOI data from Gurnett et al. (2005). Third, with the twelve new radio occultation profiles of Saturn's equatorial ionosphere taken by Cassini indicating a dawn-dusk asymmetry, Moore et al. (2006) found that a topside water influx of $\sim 5 \times 10^6\,\text{H}_2\text{O}\,\text{cm}^{-2}\,\text{s}^{-1}$ provided the best fit to the averaged dawn and dusk Cassini profiles, thereby reducing the importance of vibrationally excited H_2 as an atomic-to-molecular-ion catalyst. Finally, Moore and Mendillo (2007) included time-dependent neutral water diffusion calculations in which the topside water flux is increased for a short period of time leading to a bulge of water density that reduces the local electron density as it diffuses downward. They obtained a "temporary bite-out" similar to the observed one, as shown in Fig. 8.11. However, such a large water influx (their particular simulation used an augmentation of the background water flux $\left(5 \times 10^6\,\text{cm}^{-2}\,\text{s}^{-1}\right)$ by a factor of 50, that persisted for $\sim 27\,\text{min}$) has not yet been observed, so one cannot draw definitive conclusion at this time. On the other hand there were only two such large bite-outs observed among the 27 occultations presented here, so one needs such large fluxes only "intermittently".

Matcheva et al. (2001) examined the potential role of gravity waves as the mechanism responsible for large and sharp electron density layering, as well as for the low peak electron densities observed by Galileo at Jupiter. They pointed out that at higher altitudes where long lived H^+ dominates diffusion is likely to dominate and act to limit large deviations from diffusive equilibrium. However, they also found that a downward electron flux at high altitudes produced from the long-term effects of gravity waves can reduce the electron densities throughout the middle and upper ionosphere, in a manner similar to that proposed from a water influx or vibrationally excited H_2. Moreover, Matcheva et al. (2001) showed that at Jupiter, in the altitude range of between about 600 to 900 km, gravity waves are likely to be important in creating the observed sharp, multiple density peaks. At this point without a more detailed quantitative calculation for conditions at Saturn, it is impossible to come to a definitive conclusion regarding the observed bite-out observed by Cassini (Fig. 8.8b). As indicated in Fig. 8.8b the very large bite-out is at 2,000 km where H^+ is likely to be a major ion and thus diffusion lifetimes are significant. Therefore, such a large perturbation is less likely to be caused by gravity waves; on the other hand the smaller bite-outs seen in many of the observed electron density profiles around 1,000 km could certainly be caused by the mechanism proposed by Matcheva et al. (2001).

The models mentioned so far predict that the dominant ions in Saturn's ionosphere are H^+ and H_3^+. H_2^+ is the ion with the greatest rate of photo-production, yet it is rapidly converted to H_3^+ (Eq. 8.3), and therefore no appreciable density of H_2^+ remains. The fast dissociative recombination of H_3^+ means that it has a strong diurnal variation, with a minimum just
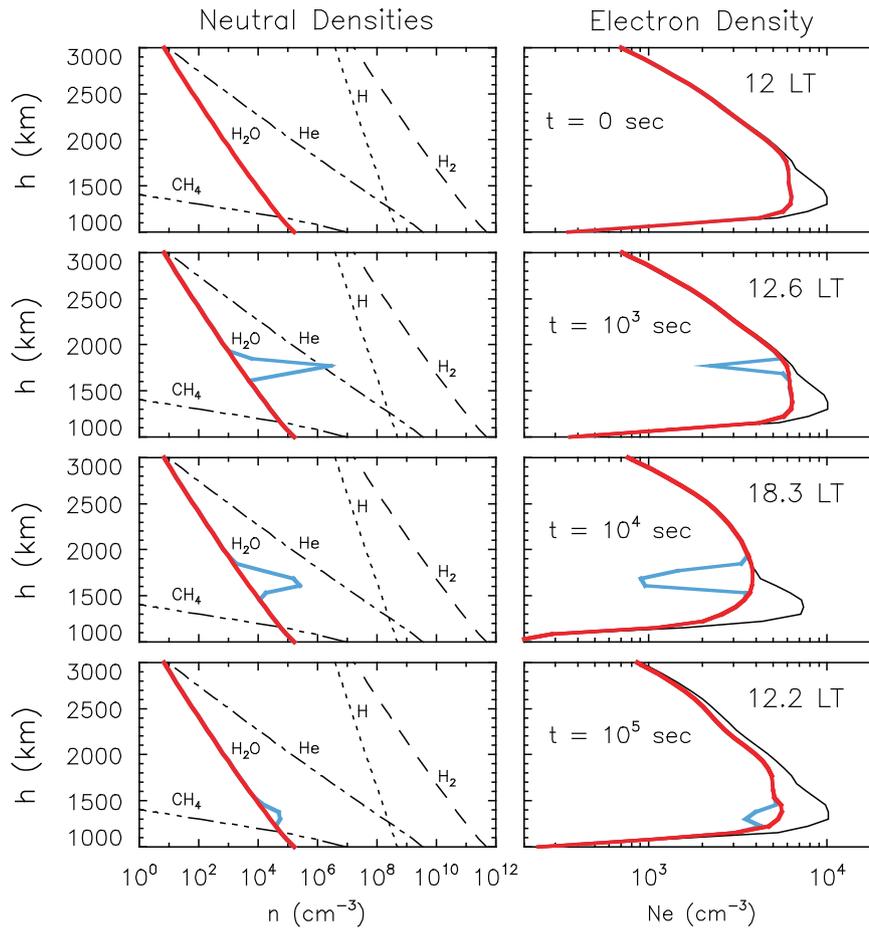
Fig. 8.11 Time evolution of a water surge simulation at Saturn. Black curves represent the nominal atmosphere for which $[H_2O] = 0$, red curves correspond to an atmosphere for which there is a constant top-side water influx of 5×10^6 H_2O molecules s^{-1}, and blue curves present the result of a surge in the topside water influx equivalent to an augmen- tation in the background by a factor of 50 persisting for 1,600 s. Similar ionospheric "bite-outs" can result from lesser augmentations over longer durations. For radio occultation observations of such structure refer to Section 8.5 (from Moore and Mendillo 2007)

before sunrise. These models also indicated that the losses for H^+ are relatively slow, and thus it has a much milder diurnal variation that is dependent on the local populations of H_2O and vibrationally excited H_2. Finally, they all predict that H_3^+ is the dominant ion near and below the electron density peak during the day, while H^+ is the dominant ion for all local times above the peak, and certainly in the topside ionosphere and at night. Moore et al. (2004) show that the expected relative distribution of H^+ and H_3^+ vary with latitude and season. The lower ionosphere is dominated by a complicated assortment of hydrocarbon ions, of which $C_3H_5^+$ is the most numerous in the model of Moses and Bass (2000).

More recently Hallett et al. (2005a) and Shemansky et al. (2009) describe comprehensive calculations in which they track the physical state of the non-LTE environment and weakly ionized plasma that would develop in a pure H_2 atmosphere under conditions relevant to the upper atmosphere of Saturn. They are able to obtain electron densities consistent with observations without including H_2O, as a loss

mechanism for H^+. Their 1D chemical/diffusive model uses a modified Monte Carlo approach and predicts that H_3^+ is the dominant ion throughout the Saturn ionosphere up to about 2,000 km, in agreement with previous models (see Fig. 8.10b). The conclusions of Shemansky et al. (2009) are partially the result of a more realistic calculation of the vibration/rotation state of the H_2 in a pure hydrogen system that includes electron forcing (Eq. 8.6) and of the new rates that they have obtained and used for the reaction of H^+ with H_2 (Eq. 8.5). Yet, as water has been observed at Saturn by ISO (Feuchtgruber et al. 1997), Hubble (Prangé et al. 2006), and now Cassini (Bjoraker et al. 2008), it is clear that the balance between the water and non-water H^+ loss pathways remains to be determined.

Shemansky et al. (2009) highlight the importance of the electron populations in controlling the activation of ground-state H_2. Most Saturn ionospheric density models to date have ignored photoelectrons, electron impact processes, electron scattering and vibrational excitation/relaxation, and

have focused on solar photon processes alone. Neglect of the electron population may also be one cause of the model-data mismatches discussed above. Note that both Shemansky et al. (2009) and Huestis (2008) point out that reaction (8.5) can lead to vibrational relaxation of H_2 as well as charge-exchange, with Huestis (2008) indicating that it is likely to be the dominant process. On the other hand Shemansky et al. (2009) maintain that the energy gained by H^+, will deliver its energy back to H_2 and into vibrational excitation. Furthermore, Shemansky et al. (2009) also indicate that in their model they do not include the critically important momentum transfer and vibrational excitation reaction of the hot atomic hydrogen product with H_2 (X) (Hallett et al. 2005b), because of the lack of the appropriate collision matrix, and thus their vibrational excitation values are lower limits. The topic of the non-LTE state of the H_2 is clearly one with important and unresolved implications for upper atmospheric research at Saturn, Jupiter, and the hydrogen-rich atmospheres of other giant planets.

Galand et al. (2009) have shown that electron impact ionization by photoelectrons and secondaries is a significant ionization process in the bottomside sunlit ionosphere, increasing the electron density by a factor of ∼2–10 over calculations that ignore secondary production below about 1,100 km. Based on the work of Galand et al. (2009), a parameterization of the secondary ionization production rate at Saturn has been developed by Moore et al. (2009).

8.6.3 Plasma Temperatures in Saturn's Ionosphere

As in the case of other ionospheric processes, such as chemistry and dynamics, plasma temperature calculations at Saturn draw heritage from terrestrial and Jovian studies. Prior to 2007, there was only one published theoretical determination of ion and electron temperatures in Saturn's ionosphere (Waite 1981). However, as those calculations were performed using a now known to be unrealistic neutral temperature profile with an exospheric temperature of nearly 1,000 K (see discussion in Section 8.2), a new derivation based on more recent spacecraft data and laboratory rates was warranted. Waite (1981) predicted ion and electron temperatures ranging from 1,000 K to 100,000 K, depending on the values of various assumed parameters, such as ion-neutral differential velocities (leading to Joule heating) and downward heat fluxes at the upper boundary. Two new studies of plasma temperatures in Saturn's ionosphere were published recently. The first focused on high latitudes and used a one-dimensional multi-fluid model to study the polar wind at Saturn (Glocer et al. 2007). Glocer et al. mod-

eled the ionosphere from below the peak to an altitude of one Saturn radius, yielding densities, fluxes and temperatures for H_3^+ and H^+. They calculated densities of a few time $10^4 \, cm^{-3}$ which are consistent with the Voyager and Cassini results. Calculated fluxes of outflowing ions over the polar cap were estimated to be in the range from 2.1×10^{26} to $7.5 \times 10^{27} \, s^{-1}$, making Saturn's auroral ionosphere an intermediate source of magnetospheric plasma, larger than the Titan Torus source (Smith et al. 2004), and smaller than the icy satellite source (e.g., Jurac and Richardson 2005). Finally, the calculated peak ion temperatures varied from about 1,500 to 3,000 K.

The second recent study of plasma temperatures in Saturn's ionosphere used STIM as a basis for the calculations (Moore et al. 2008), and focused on the low- and mid-latitude ionosphere, neglecting auroral energy inputs as well as potential energy storage at high altitudes in the field tubes. Three codes were coupled sequentially in order to derive self-consistent time-dependent ion and electron temperatures: (1) the STIM thermosphere discussed above (Müller-Wodarg et al. 2006), (2) the 1D STIM ionospheric module (Moore et al. 2004), and (3) a suprathermal electron transport code adapted to Saturn (Galand et al. 1999, 2006). Moore et al. (2008) predicted topside electron temperatures to range between 500–560 K (∼80–140 K above the neutral temperature). After sunset, plasma-neutral interactions quench the electron gas within two Saturn hours. Ion temperatures, calculated for only the major ions H^+ and H_3^+, were somewhat smaller, reaching ∼480 K during the day at the topside while remaining nearly equal to the neutral temperature at altitudes near and below the N_e peak. For easy reference, Table 8.1 provides a partial timeline of papers describing models of Saturn's ionosphere.

8.7 Summary

If the Cassini observations with respect to the upper atmosphere and ionosphere of Saturn were to be summarized with one main theme, that theme would be *variability*. The Cassini UVIS observations of the neutral upper atmosphere and the radio-science observations of the ionosphere emphasize that Saturn's upper atmosphere is much more temporally and spatially variable than has generally been realized from the Voyager observations.

The preliminary Cassini UVIS δ-Ori stellar occultation results (Shemansky and Liu 2009) imply a thermospheric temperature that is ∼140–180 K colder than temperatures inferred from a reanalysis of all six Voyager UVS occultations (Vervack and Moses 2009). Both the new Cassini data and the Voyager reanalyses suggest that thermospheric neutral temperatures on Saturn are of order 300–500 K and not as large as 800 K. However, even these 300–500 K temperatures

Table 8.1 Models of Saturn's ionosphere

Author(s)	Transport	N_{MAX} (cm^{-3})	h_{MAX} (km)	Comments (k = H$^+$ + H$_2$ ($v \geq 4$) reaction rate)
McElroy (1973)	No	30	120	Altitude referenced to the homopause. Does not include H$^+$ + H$_2$ ($v \geq 4$) reaction.
Atreya and Donahue (1975)	No	10	300	Introduced hydrocarbon chemistry to lower ionosphere. Altitudes referenced to the [H$_2$] = 10^{16} cm^{-3} level.
Capone et al. (1977)	No	30	680	Lower electron peak of 7×10^3 cm^{-3} at 50 km due to cosmic-ray ionization.
Waite et al. (1979)	Yes	10	2,000	Altitudes referenced to the [n] = 10^{19} cm^{-3} level. Assumed an exospheric temperature of 1,300 K and an eddy diffusion coefficient of 1.3 $\times 10^6$ cm^2 s^{-1}.
Waite (1981)	Yes	10	1,200	For an eddy diffusion coefficient of 10^6 cm^2 s^{-1}. Also calculated plasma temperatures for a 1,000 K neutral exospheric temperature.
Majeed and McConnell (1991)	Yes	1	2,200	Nominal model N_{MAX} of 3×10^5 cm^{-3} at 1,200 km. Quoted values use either $\Phi_{H_2O} = 2.2 \times 10^7$ cm^{-2} s^{-1} and $k = 0$, or $\Phi_{H_2O} = 0$ and $k = 1.38 \times 10^{-14}$ cm^3 s^{-1}
Majeed and McConnell (1996)	Yes	2	1,800	For $\Phi_{H_2O} = 10^7$ cm^{-2} s^{-1} and $k = 0$. Also explores more values of Φ_{H_2O} and k in a time-dependent ionosphere.
Moses and Bass (2000)	Yes	1	1,400	Time-dependent solution for 46 ion species. Explores water and metal influx from ring or meteoric sources. Neutral wind and electric field induced plasma motions studied.
Moore et al. (2004)	Yes	1	1,400	Global solution using 3D thermosphere. Investigation of ring shadowing. Ionospheric conductivities.
Moore et al. (2006); Moore and Mendillo (2007)	Yes	0.1 dawn/0.4 dusk	2,500 dawn/ 1,900 dusk	Parameter space exploration of H$_2$O and k in order to reproduce average Cassini behavior. Time-dependent neutral water diffusion calculations leading to ionospheric "bite-outs".
Glocer et al. (2007)	Yes	0.3–2	1,400–3,000	Polar wind steady-state study (1 R$_S$ upper boundary). Includes plasma temperatures. Wide range of T$_{exo}$ explored.
Moore et al. (2008)	Yes	0.4 dawn/1 dusk	1,600 dawn/ 1,300 dusk	Plasma temperature calculations. Water influx. Voyager 2 era rather than Cassini (as in Moore et al., 2006).
Shemansky and Liu (2009)	Yes	2	1,100	Complete non-LTE calculations of the pure H$_2$ environment of Saturn; major ion is H$_3$$^+$ up to 2,000 km.

are higher than can be explained by the absorption of solar extreme ultraviolet radiation alone, and the thermospheric heat sources on Saturn have yet to be explained. Modeling, such as is described in Section 8.4, can help provide clues to the dominant heating mechanisms.

In retrospect, the older Voyager data also suggest variability in upper atmospheric structure on Saturn, especially with regard to the hydrocarbon abundance profiles and the location of the methane homopause (e.g., Vervack and Moses 2009), but because the Voyager ultraviolet occultation data have only been analyzed in a full and consistent manner recently, this variability was not recognized. Unlike the earlier Voyager view of vigorous atmospheric mixing in Saturn's stratosphere, the Cassini UVIS δ-Ori stellar occultation results (Shemansky and Liu 2009) imply a very low-

altitude methane homopause at −42.7 latitude, suggesting that atmospheric mixing is relatively weak or downward vertical winds are affecting the methane profile in Saturn's middle atmosphere at this location and time. The overall variability in all the ultraviolet occultations to date suggests that vertical winds play a major role in controlling the methane profile in the homopause region on Saturn, and it is hoped that analysis of the numerous as-yet-to-be examined Cassini UVIS occultations may help constrain middle-atmospheric circulation on Saturn. Current photochemical models based on the neutral chemistry described in Moses et al. (2005) do not accurately reproduce the overall shape of the hydrocarbon vertical profiles derived from the ultraviolet occultations, and further investigation into possible reasons for the model-data mismatch are warranted. Constraints on both vertical

transport and upper-atmospheric chemistry are likely to be derived from such model-data comparisons.

Although ultraviolet occultations remain one of the few techniques for which we can obtain information on thermospheric temperatures and neutral species abundances, one must keep in mind that the derived results are almost always very model dependent. Analysis and modeling techniques have improved tremendously since the early Voyager analyses, but uncertainties and poorly constrained model parameters remain that can complicate the derivations.

The Cassini radio occultation electron density profiles have significantly increased our data base. We now have good latitudinal coverage of electron densities. The diurnal variations in the peak electron densities inferred by the new Cassini SED observations are large and similar to the ones from Voyager. Significant progress has also been made in modeling the ionosphere. These new observations and models are welcome; however, there is still a lot we do not know nor understand about Saturn's ionosphere. Ion composition is one important issue without a definitive resolution. Electron density measurements can provide some indirect clues on the ion composition, but no definitive information. There appears to be agreement that H_3^+ is the dominant ion at the lower altitudes and H^+ is the major ion at the higher altitudes. The relative importance of vibrationally excited H_2 compared to water inflow or gravity waves in removing H^+ is still being debated. The scale height derived sub-auroral plasma temperatures have very large uncertainties and appear to be higher than the corresponding model values. Unfortunately, as long as the only data we have to work with are scale heights from topside electron density profiles, we will have to live with these uncertainties. Improved models will hopefully help to elucidate some of the issues associated with these parameters that are not being measured directly. The large variability in the electron densities observed from radio occultation profiles at similar latitudes and times suggests that dynamical and/or electrodynamical processes play a major role in controlling ionospheric structure on Saturn; such processes should be investigated in future models to the extent that is possible.

Note added in proof: The UVIS occultation results presented in this chapter were based on a preliminary analysis; some of the results have changed. See Shemansky and Liu (2009) for the updated results.

References

Atreya, S. K. and T. M. Donahue, The role of hydrocarbons in the ionospheres of the outer planets, *Icarus, 25*, 335–338, 1975.

Atreya, S. K., T. M. Donahue, and J. H. Waite Jr., An interpretation of the Voyager measurement of Jovian electron density profiles, *Nature, 280*, 795–796, 1979.

Atreya, S. K., J. H. Waite, Jr., T. M. Donahue, A. F. Nagy, J. C. McConnell, Theory, measurements, and models of the upper atmosphere and ionosphere of Saturn. In: Gehrels, T., Matthews, M.S. (Eds.), *Saturn*, Univ. Arizona Press, Tucson, pp. 239–277, 1984.

Baron R. L., R. D. Joseph, T. Owen, J. Tennyson, S. Miller, and G. E. Ballester, Infrared imaging of H_3^+ in the ionosphere of Jupiter, *Nature, 353*, 539–542, 1991.

Bezard, B., J. J. Moses, J. Lacy, T. Greathouse, M. Richter, and C. Griffith, Detection of ethylene C_2H_4 on Jupiter and Saturn in non-auroral regions, *Bull. Am. Astron. Soc., 33*, 1079–1080, 2001.

Bjoraker, G.L., R.K. Achterberg, A.A. Simon-Miller, R.C. Carlson, and D.E. Jennings, Cassini/CIRS observations of water vapor in Saturn's stratosphere, *Saturn After Cassini-Huygens*, Imperial College, London, 28 July–1 August, 2008.

Broadfoot, A.L., and 15 co-authors, Extreme ultraviolet observations from Voyager 1 encounter with Saturn, *Science, 212*, 206–211, 1981.

Capone, L. A., R. C. Whitten, S. S. Prasad, and J. Dubach, The ionospheres of Saturn, Uranus, and Neptune, *Astrophys. J., 215*, 977–983, 1977.

Connerney, J. E. P. and J.H. Waite Jr., New model of Saturn's ionosphere with an influx of water from the rings, *Nature, 312*, 136–138, 1984.

Connerney, J. E. P., Magnetic connection for Saturn's rings and atmosphere, *Geophys. Res. Lett., 13*, 773, 1986.

Courtin, R., D. Gautier, A. Marten, B. Bezard, and R. Hanel, The composition of Saturn's atmosphere at northern temperate latitudes from Voyager IRIS spectra: NH_3, PH_3, C_2H_2, C_2H_6, CH_3D, CH_4, and the Saturnian D/H isotopic ratio, *Astrophys. J., 287*, 899–916, 1984.

Cowley S. W. H., E.J. Bunce, and R. Prange, Saturn's polar ionospheric flows and their relation to the main auroral oval. *Ann. Geophys., 22*, 1379–1394, 2004.

Cravens, T. E., Vibrationally excited molecular hydrogen in the upper atmosphere of Jupiter, J. *Geophys. Res., 92*, 11083, 1987.

Drossart P., J-P. Maillard, J. Caldwell, S. J. Kim, J. K. G. Watson, W. A. Majewski, J. Tennyson, S. Miller, S. K. Atreya, J. T. Clarke, J. H. Waite Jr, and R. Wagener, Detection of H_3^+ on Jupiter, *Nature, 240*, 539–541, 1989.

Dungey J. W., The interplanetary magnetic field and auroral zones. *Phys. Rev. Lett., 6*, 47, 1961.

Dyudina, U. A., A. P. Ingersoll, P. E. Shawn, C. C. Porco, G. Fischer, W. S. Kurth, M. D. Desch, A. Del Genio, J. Barbara, and J. Ferrier, Lightning storms on Saturn observed by Cassini ISS and RPWS in the years 2004–2006, *Icarus, 190*, 545–555, 2007.

Esposito, L. W., et al, The Cassini ultraviolet imaging spectrograph investigation, *Space Sci. Rev., 115*, 299–361, 2004.

Festou M. C. and S. K. Atreya, Voyager ultraviolet stellar occulation measurements of the composition and thermal profiles of the saturnian upper atmosphere, *Geophys. Res. Lett*., 9, 1147–1152, 1982.

Festou, M. C., S. K. Atreya, T. M. Donahue, B. R. Sandel, D. E. Shemansky, and A. L. Broadfoot, Composition and thermal profiles of the Jovian upper atmosphere determined by the Voyager ultraviolet stellar occultation experiment, *J. Geophys. Res., 86*, 5715–5725, 1981.

Feuchtgruber, H., E. Lellouch, T. de Graauw, B. Bézard, T. Encrenaz, and M. Griffin, External supply of oxygen to the atmospheres of the giant planets, *Nature, 389*, 159–162, 1997.

Flasar, F. M., et al., Temperatures, winds and composition in the Saturnian system, *Science*, 307, 1247–1251, doi: 10.1126/science.1105806, 2005.

Fischer, G. et al., Atmospheric electricity at Saturn, *Space Sci. Rev., 137*, 271–285, doi:10.1007/s11214–008–9370-z, 2008.

Fletcher, L. N., et al., Characterizing Saturn's vertical temperature structure from Cassini/CIRS, *Icarus, 189*, 457–478, 2007.

Fouchet, T., et al.: Saturn composition and chemistry. Chapter 5, this book, 2009.

Geballe T.R., M.-F. Jagod, and T. Oka, Detection of H_3^+ infrared emission lines in Saturn, *Astrophys. J.*, 408, L109–L112, 1993.

Galand, M., J. Lilensten, D. Toublanc, and S. Maurice, The ionosphere of Titan: Ideal diurnal and nocturnal cases, *Icarus, 140*, 92–105, 1999.

Galand, M., R.V. Yelle, A. J. Coates, H. Backes, and J.-E. Wahlund, Electron temperature of Titan's sunlit ionosphere, *Geophys. Res. Lett., 33*, L21101, doi:10.1029/2006GL0247488, 2006.

Galand, M., L. Moore, B. Charney, I. C. F. Müller-Wodarg, and M. Mendillo, Solar primary and secondary ionization at Saturn, *J. Geophys Res., 114*, A06313, doi:10.1029/2008JA013981, 2009.

Glocer, A., T. I. Gombosi, G. Toth, K. C. Hansen, A.J. Ridley, and A. Nagy, Polar wind outflow model: Saturn results, *J. Geophys. Res., 112*, doi:10.1029/2006JA011755, 2007.

Greathouse, T. K., J. H. Lacy, B. Bezard, J. I. Moses, C. A. Griffith, and M. J. Richter Meridional variations of temperature, C_2H_2 and C_2H_6 abundances in Saturn's stratosphere at southern summer solstice, *Icarus, 177*, 18–31, 2005.

Gurnett, D. A., et al., Radio and plasma wave observations at Saturn from Cassini's approach and first orbit, *Science, 307*, 1255–1259, 2005.

Hallett, J. T., D. E. Shemansky, and X. Liu, A rotational-level hydrogen physical chemistry model for general astrophysical application. *Astrophys. J., 624*, 448–461, 2005a.

Hallett, J. T., D. E. Shemansky, and X. Liu, Fine-structure physical chemistry modeling of Uranus H2 X quadrupole emission, *Geophys. Res. Lett., 32*, L02204, doi:10.1029/2004GL021327, 2005b.

Hubbard, W. B. and 27 colleagues, Structure of Saturn's mesosphere from the 28 Sgr occultations. *Icarus, 130*, 404–425, 1997.

Huestis, D. L., Hydrogen collisions in planetary atmospheres, ionospheres, and magnetospheres, *Planet. Space Sci., 56*, 1733, 2008.

Ichihara, A., O. Iwamoto, and R. K. Janev, 2000, Cross sections for the reaction $H^+ + H_2 (v = 0 - 14) - > H + H_2^+$, *J. Phys. B, 33*, 4747, 2000.

Isbell J., A. J. Dessler, and J. H. Waite, Magnetospheric energisation by interaction between planetary spin and the solar wind, *J. Geophys. Res., 89*, 10716–10722, 1984.

Kaiser, M. L., J. E. P. Connerney, and M. D. Desch, Atmospheric storm explanation of saturnian electrostatic discharges, *Nature, 303*, 50–53, 1983.

Jurac, S. and J.D. Richardson, A self-consistent model of plasma and neutrals at Saturn: Neutral cloud morphology, *J. Geophys. Res., 110*, A09220, doi:10.1029/2004JA010635, 2005.

Kaiser, M. L., M. D. Desch, and J. E. P. Connerney, Saturn's ionosphere – Inferred electron densities, *J. Geophys. Res., 89*, 2371–2376, 1984.

Killen, R., D.E. Shemansky, and N. Mouawad, Expected emission from Mercury's exospheric species, and their UV-Visible signatures, *Ap. J. Suppl., 181*, 351, 2009.

Kliore, A. J., J. D. Anderson, J. W. Armstrong, S. W. Asmar, C. L. Hamilton, N. J. Rappaport, H. D. Wahlquist, R. Ambrosini, F. M. Flasar, R. G. French, L. Iess, E. A. Marouf, and A. F. Nagy, Cassini Radio Science, *Space Sci. Rev., 115*, 1–70, 2004.

Kliore, A. J., et al., Midlatitude and high-latitude electron density profiles in the ionosphere of Saturn obtained by Cassini radio occultation observations. *J. Geophys. Res., 114*, A04315, doi:10.1029/2008JA0139000, 2009.

Lam H. A., N. Achilleos, S. Miller, J. Tennyson, L. M. Trafton, T. R. Geballe, and G. Ballester, A baseline spectroscopic study of the infrared aurorae of Jupiter, *Icarus, 127*, 379–393, 1997.

Lindal, G. F., D. N. Sweetnam, and V. R. Eshleman, The Atmosphere of Saturn: An Analysis of the Voyager Radio Occultation Measurements, *Astron. J., 90*, 1136–1146, 1985.

Lindal, G. F., The atmosphere of Neptune: An analysis of radio occultation data acquired with Voyager 2, *Astron. J., 103*, 967–982, 1992.

Majeed, T. and J. C. McConnell, The upper ionospheres of Jupiter and Saturn, *Planet. Space Sci., 39*, 1715–1732, 1991.

Majeed, T., R. V. Yelle, and J. C. McConnell, Vibrationally excited H_2 in the outer planet thermospheres – Fluorescence in the Lyman and Werner bands, *Planet. Space Sci., 39*, 1591–1606, 1991.

Majeed, T. and J. C. McConnell, Voyager electron density measurements on Saturn: Analysis with a time dependent ionospheric model, *J. Geophys. Res., 101*, 7589–7598, 1996.

Matcheva, K.I., D.F. Strobel, and F.M. Flasar, Interaction of gravity waves with ionospheric plasma: Implications for Jupiter's ionosphere, *Icarus, 152*, 347–365, doi:10.1006/Icar.2001.6631, 2001.

McConnell, J. C., J. B. Holberg, G. R. Smith, B. R. Sandel, D. E. Shemansky, and A. L. Broadfoot, A new look at the ionosphere of Jupiter in light of the UVS occultation results, *Planet. Space Sci., 30*, 151–167, 1982.

McElroy, M. B, The ionospheres of the major planets, *Space Sci. Rev., 14*, 460–473, 1973.

Melin, H., S. Miller, T. Stallard, C. Smith, and D. Grodent, Estimated energy balance in the jovian upper atmosphere during an auroral heating event, *Icarus, 181*, 256–265, doi:10.1016/j.icarus.2005.11.004, 2006.

Melin, H., S. Miller, T. Stallard, L. M. Trafton, and T. R. Geballe, Variability in the H_3^+ emission from Saturn: consequences for ionisation rates and temperature, *Icarus, 186*, 234–241, 2007.

Melin, H., D. E. Shemansky, and X. Liu, The distribution of atomic hydrogen and oxygen in the magnetosphere of Saturn, *Planet. Space Sci.*, doi: 101016/j.pss2009.04.014, 2009.

Mendillo, M., L. Moore, J. Clarke, I. Müller-Wodarg, W.S. Kurth, and M.L. Kaiser, Effects of ring shadowing on the detection of electrostatic discharges at Saturn, *Geophys. Res. Lett., 32*, L05107, doi:10.1029/2004GL021934, 2005.

Miller S., H.A. Lam, and J. Tennyson, What astronomy has learned from observations of H_3^+, *Can. J. Phys.*, 72, 760–771, 1994.

Miller S. and 10 others, The role of H3+ in planetary atmospheres, *Phil. Trans. Roy. Soc.* 358, 2485–2502, 2000.

Miller S., A. Aylward, and G. Millward, Giant planet ionospheres and thermospheres: The importance of ion-neutral coupling, *Space Sci. Rev., 116*, 319–343, 2005.

Miller S., T. Stallard, C. Smith, G. Millward, H. Melin, M. Lystrup, and A. Aylward, H_3^+: the driver of giant planet atmospheres, *Phil. Trans. Roy. Soc., 364*, 3121–3138, 2006.

Moore, L. and M. Mendillo, Ionospheric contribution to Saturn's inner plasmasphere, *J. Geophys. Res., 110*, A05310, doi:10.1029/2004JA010889, 2005.

Moore, L. and M. Mendillo, Are plasma depletions in Saturn's ionosphere a signature of time-dependent water input?, *Geophys. Res. Lett., 34*, L12202, doi:10.1029/2007GL029381, 2007.

Moore, L. E., M. Mendillo, I. C. F. Müller-Wodarg and D. L. Murr, Modeling of global variations and ring shadowing in Saturn's ionosphere, *Icarus, 172*, 503–520, 2004.

Moore, L., A. F. Nagy, A. J. Kliore, I. Müller-Wodarg, J. D. Richardson and M. Mendillo, Cassini radio occultations of Saturn's ionosphere: Model comparisons using a constant water flux, *Geophys. Res. Lett., 33*, L22202, 2006.

Moore, L., M. Galand, I. Müller-Wodarg, R. Yelle, and M. Mendillo, Plasma temperatures in Saturn's ionosphere, *J. Geophys. Res., 113*, A10, A10306, 10.1029/2008JA013373, 2008.

Moore, L., M. Galand, I. Müller-Wodarg, and M. Mendillo, Response of Saturn's ionosphere to solar radiation: Testing parameterizations for thermal electron heating and secondary ionization processes, *Planet. Space Sci.*, doi:10.1016/j.pss.2009.05.001, 2009.

Moses, J.I. and S.F. Bass, The effects of external material on the chemistry and structure of Saturn's ionosphere, *J. Geophys. Res., 105*, 7013–7052, 2000.

Moses, J. I., B'ezard, B., Lellouch, E., Gladstone, G. R., Feuchtgruber, H., Allen, M., Photochemistry of Saturn's atmosphere. I. Hydrocarbon chemistry and comparisons with ISO observations. *Icarus, 143*, 244–298, 2000.

Moses, J. I., T. Fouchet, R. V. F. Yelle, A. J. Friedson, G. S. Orton, B. B'ezard, P. Drossart, G. R. Gladstone, T. Kostiuk, T. A. Livengood, The stratosphere of Jupiter. In: Bagenal, F., Dowling, T.E., McKinnon, W.B. (Eds.), *Jupiter: The Planet, Satellites and Magnetosphere*, Cambridge University Press, Cambridge, UK, pp. 129–157, 2004.

Moses, J. I., T. Fouchet, B. B'ezard, G. R. Gladstone, E. Lellouch, H. Feuchtgruber, Photochemistry and diffusion in Jupiter's stratosphere: Constraints from ISO observations and comparisons with other giant planets, *J. Geophys. Res., 110*, E08001, doi:10.1029/2005JE002411 2005.

Moses, J. I. and R. J. Vervack, Jr., The structure of the upper atmosphere of Saturn, *Lunar Planet. Sci. Conf., 37*, #1803, 2006.

Müller-Wodarg, I. C. F., M. Mendillo, R. V. Yelle, and A. D. Aylward, A global circulation model of Saturn's thermosphere, *Icarus, 180*, 147–160, 2006.

Nagy, A. F., A. J. Kliore, E. Marouf, R. French, M. Flasar, N. Rappaport, A. Anabtawi, S. W. Asmar, D. Johnston, E. Barbinis, and 2 coauthors, First results from the ionospheric radio occultations of Saturn by the Cassini spacecraft, *J. Geophys. Res., 111*, A06310, 2006.

Pierrard, V. and J. Lemaire, Lorentzian ion exosphere model, *J. Geophys. Res., 101*, 7923–7934, 1996.

Pierrard, V. and J. Lemaire, Erratum: Lorentzian ion exosphere model, *J. Geophys. Res., 101*, 7923–7934, 1996; 103, 4117–4118, 1998.

Prangé, R., T. Fouchet, R. Courtin, J.E.P. Connerney, and J.C. McConnell, Latitudinal variation of Saturn photochemistry deduced from spatially-resolved ultraviolet spectra, *Icarus*, 180, 379–392, 2006.

Sada, P. V., G. L. Bjoraker, D. E. Jennings, P. N. Romani, and G. H. McCabe, Observations of C2H6 and C2H2 in the stratosphere of Saturn, *Icarus 173*, 499–507, 2005.

Sandel, B.R., and 12 co-authors, Extreme ultraviolet observations from the Voyager 2 encounter with Saturn, *Science, 215*, 548–553, 1982.

Schunk, R. W. and A. F. Nagy, *Ionospheres*, 2nd edn, Cambridge University Press, 2009.

Shemansky, D. E. and D. T. Hall, The distribution of atomic hydrogen in the magnetosphere of Saturn, *J. Geophys. Res., 97*, 4143–4161, 1992.

Shemansky, D. E., A. I. F. Stewart, R. A. West, L. W. Esposito, J. T. Hallett, and X. M. Liu, The Cassini UVIS Stellar probe of the Titan atmosphere, *Science, 308*, 978, 2005.

Shemansky, D. E., X. Liu, and H. Melin, The Saturn hydrogen plume, *Planet. Space Sci.*, doi:101016/j.pss2009.05.002, 2009.

Shemansky, D. E. and X. Liu, Saturn upper atmospheric structure from Cassini EUV/FUV occultations, *Planet. Space Sci.*, under review, 2009.

Smith, G. R., D. E. Shemansky, J. B. Holberg, A. L. Broadfoot, B. R. Sandel, Saturn's upper atmosphere from the Voyager 2 EUV solar and stellar occultations, *J. Geophys. Res. 88*, 8667–8678, 1983.

Smith, G. R. and D. M. Hunten, Study of planetary atmospheres by absorptive occultations, *Rev. Geophys., 28*, 117, 1990.

Smith, H.T., R.E. Johnson, and V.I. Shematovich, Titan's atomic and molecular nitrogen tori, *Geophys. Res. Lett.*, 31 L16804, doi:10.1029/2004GL020580, 2004.

Smith, C. G. A., A. D. Miller, S., Müller-Wodarg, I. C. F., Polar heating in the Saturn's thermosphere, *Ann. Geophys., 23*, 2465–2477, 2005.

Smith C. G. A., A. D. Aylward, G. H. Millwrad, S. Miller and L. Moore, An unexpected cooling effect in Saturn's upper atmosphere, *Nature, 445*, 399–401, 2007.

Stallard T., S. Miller, G. E. Ballester, D. Rego, R. D. Joseph, and L. M. Trafton, The H$_3$$^+$ latitudinal profile of Saturn, Astrophys. *J. Lett., 521*, L149–L152, 1999.

Stallard, T., S. Miller, L. M. Trafton, T. R. Geballe, R. D. Joseph, Ion winds in Saturn's southern auroral/polar region, *Icarus, 167*, 204–211, 2004.

Stallard T., et al., Complex structure within Saturn's infrared aurora, *Nature, 456*, 214, 2008.

Strobel, D. F. and G. R. Smith, On the temperature of the Jovian thermosphere, *J. Atm. Sci., 30*, 718, 1973.

Strobel, D. F., Photochemistry in outer solar system atmospheres, *Space Sci. Rev., 116*, 155–170, 2005.

Trafton L. M., T. R. Geballe, S. Miller, J. Tennyson, and G.E. Ballester, Detection of H$_3^+$ from Uranus, *Astrophys. J., 405*, 761–766, 1993.

Vasyliunas V. M., Plasma distribution and flow. In: Dessler A.J. (ed.), *Physics of the Jovian Magnetosphere*, Cambridge University Press, pp. 395–453, 1983.

Vervack, R. J., Jr., and J. I. Moses, Saturn's upper atmosphere during the Voyager era: Reanalysis and modeling of the UVS occultations, *Icarus*, under review, 2009.

Waite, J. H., S. K. Atreya, and A. F. Nagy, The ionosphere of Saturn – Predictions for Pioneer 11, *Geophys. Res. Lett., 6*, 723–726, 1979.

Waite, J. H., T. E. Cravens, J. U. Kozyra, A. F. Nagy, S. K. Atreya, and R. H. Chen, Electron precipitation and related aeronomy of the Jovian thermosphere and ionosphere, *J. Geophys. Res., 88*, 6143–6163, 1983.

Waite, J.H., *The ionosphere of Saturn*, PhD Thesis, Univ. of Mich., Ann Arbor, 1981.

Warwick, J. W., D. R. Evans, J. H. Romig, J. K. Alexander, M. D. Desch, M. L. Kaiser, M. G. Aubier, Y. Leblanc, A. Lecacheux, and B. M. Pedersen, Planetary radio astronomy observations from Voyager 2 near Saturn, *Science, 215*, 582–587, 1982.

West, R. A., D. F. Strobel, M. G. Tomasko, Clouds, aerosols, and photochemistry in the Jovian atmosphere, *Icarus, 65*, 161–217, 1986.

Wu, C. Y. R., F. Z. Chen, and D. L. Judge, Measurement of temperature-dependent absorption cross sections of C2H2 in the VUV-UV region, *J. Geophys. Res, 106*, 7629, 2001.

Yelle, R. V. and S. Miller, Jupiter's thermosphere and ionosphere. In: Bagenal, F., et al. (Ed.), *Jupiter: The Planet, Satellites, and Magnetosphere*, Cambridge Univ. Press, New York, pp. 185–218, 2004.

Yelle, R. V., L. A. Young, R. J. Vervack, Jr., R. Young, L. Pfister, and B. R. Sandel, Structure of Jupiter's upper atmosphere: Predictions for Galileo, *J. Geophys. Res. 101*, 2149–2161, 1996.

Yung, Y. L. and W. B. DeMore, *Photochemistry of Planetary Atmospheres*, Oxford University Press, Oxford, 1999.